

NACA RM E52J22

6780



CHARACTERISTICS OF A CANARD-TYPE MISSILE CONFIGURATION  
WITH AN UNDERSLUNG SCOOP INLET AT MACH NUMBERS  
FROM 1.5 TO 2.0

By Evan A. Fradenburgh and Robert C. Campbell

# Lewis Flight Propulsion Laboratory

Cleveland, Ohio *UNCLASSIFIED*  
Classification cancelled (or changed to).....

By Authority of NASA TECH PUB ANNOUNCEMENT  
(OFFICER AUTHORIZED TO CHANGE)

By 10 Dec 88  
NAME AND

.....*PM3*.....  
GRADE OF OFFICER MAKING CHANGE)

*21 Mar 61* **CLASSIFIED DOCUMENT**  
 .....  
 DATE  
 This material contains information affecting the National Defense of the United States within the meaning of the espionage laws, Title 18, U.S.C., Secs. 793 and 794, the transmission or revelation of which in any manner to an unauthorized person is prohibited by law.

NATIONAL ADVISORY COMMITTEE  
FOR AERONAUTICS

# WASHINGTON

January 30, 1953

**RECEIPT SIGNATURE**  
**REQUIRED**

~~CONFIDENTIAL~~

71908/13

34



0143442

NACA RM E52J22

~~CONFIDENTIAL~~

1X

## NATIONAL ADVISORY COMMITTEE FOR AERONAUTICS

RESEARCH MEMORANDUM

## CHARACTERISTICS OF A CANARD-TYPE MISSILE CONFIGURATION

WITH AN UNDERSLUNG SCOOP INLET AT MACH NUMBERS

FROM 1.5 TO 2.0

By Evan A. Fradenburgh and Robert C. Campbell

## SUMMARY

An experimental investigation of a canard-type missile configuration with an underslung scoop inlet was conducted in the Lewis 8- by 6-foot supersonic wind tunnel at Mach numbers from 1.5 to 2.0 for a range of angles of attack, control-surface deflection angles, boundary-layer-scoop heights, and inlet mass-flow ratios. Two inlets were tested, and total-pressure surveys were made ahead of the inlet and at the diffuser exit. The Reynolds number of the investigation, based on the mean aerodynamic chord of the wing, was approximately  $8.4 \times 10^6$ .

Measurement of the external forces indicated that maximum lift-drag ratios were in excess of 5 at all test Mach numbers. The inlet mass-flow ratio and boundary-layer-scoop height had appreciable effects on the drag coefficient.

Diffuser pressure recoveries tended to increase with increasing angle of attack because of favorable effects on the boundary layer and inlet Mach number, and were less a function of boundary-layer-scoop height at positive angles than at negative angles. Recoveries were also influenced by control-surface deflection angle. At zero angle of attack and a free-stream Mach number of 2.0, maximum pressure recoveries of 0.79 and 0.83 were measured for the 25° and 30° half-cone-angle inlet configurations, respectively.

## INTRODUCTION

The performance of an aircraft configuration cannot in all cases be successfully predicted by a study only of its component parts. In general, there will be mutual interference effects between components which invalidate a simple summation of individual performances and necessitate tests of the complete aircraft.

~~CONFIDENTIAL~~

342

2747

The present investigation of a canard-type, underslung-scoop-inlet missile configuration is part of a general program of studies of complete models for the evaluation of some of the design variables of supersonic aircraft and the interference effects associated with these designs. In reference 1, performance characteristics are presented for a canard-type missile with nacelle engines mounted on vertical struts above and below the body. In reference 2, characteristics are presented for a similar configuration with nacelle engines mounted on the wing. The model of the present test utilized the same wing and canard control surface as the models of references 1 and 2, and had a similar body size and total engine tail-pipe cross-sectional area.

Test results include external forces and moments, diffuser characteristics for two inlet designs, and pressure surveys of the boundary-layer flow ahead of the inlet and of the flow at the diffuser exit. The investigation was conducted in the NACA Lewis 8- by 6-foot supersonic wind tunnel at Mach numbers of 1.5, 1.8, and 2.0 for a range of angles of attack, control-surface deflection angles, boundary-layer-scoop heights, and inlet mass-flow ratios. The Reynolds number, based on the mean aerodynamic chord of the wing, was approximately  $8.4 \times 10^6$ .

#### SYMBOLS

The following symbols are used in this report:

A	duct cross-sectional area
$A_1$	inlet area, $\frac{1}{2} \pi r_1^2$ , 23.8 sq in.
$C_D$	drag coefficient, $\frac{D}{q_0 S}$
$C_L$	lift coefficient, $\frac{L}{q_0 S}$
$C_M$	pitching-moment coefficient, $\frac{M'}{q_0 S \bar{c}}$
$\bar{c}$	mean aerodynamic chord of wing, 17.97 in.
D	drag
$H_1, H_2$	characteristic afterbody dimensions

h boundary-layer-scoop height, measured at cone tip for  $25^\circ$  inlet

K forebody shape parameter

L lift

M Mach number

M' pitching moment about station 56, 1.5 in. above reference line

m mass flow passing through main duct

$m_0$  reference mass flow,  $\rho_0 v_0 A_1$

P total pressure

p static pressure

$q_0$  free-stream dynamic pressure,  $\frac{1}{2} \rho_0 v_0^2$

$r_1$  inlet radius, 3.89 in.

S wing plan-form area including portion blanketed by body,  
900 sq in.

v velocity

x,y coordinates normal to body reference line

$\alpha$  angle of attack

$\delta_c$  canard control-surface deflection angle measured from body  
reference line, positive when trailing edge is down

$\rho$  mass density

## Subscripts:

0 free stream

2 diffuser exit (station 108)

3 tail pipe (station 120)

e engine center line

i inlet

ind indicated

## APPARATUS AND PROCEDURE

A sketch of the model and support strut is shown in figure 1 and a photograph of the model installed in the tunnel test section appears in figure 2. The cross-sectional shape of the body was approximately circular near the nose, transforming into a flat-bottomed section rearward to accommodate the semicircular inlet. Dimensions of the body-engine are given in table I.

The wing had a total plan-form area of 900 square inches, an aspect ratio of 3, a taper ratio of 0.5, and an unswept 50-percent chord line. The airfoil section of the wing was a double circular arc, 5 percent thick. The canard control surface was geometrically similar in plan form to the wing with a total plan area of 15 percent of the wing area. The airfoil section of the canard control surface was a double circular arc 5 percent thick, except near the root where the thickness was increased to 8 percent for strength. The remotely operated control surface was all-movable and hinged about its 50-percent chord line. The nose portion of the body adjacent to the forward half of the surface was fixed to and deflected with the surface.

A variable boundary-layer-scoop height was provided by a remotely operated, movable portion of the underside of the body. This ramp, which was hinged at its forward end, projected into the air stream relative to the rest of the body in its lowest position ( $h = 0$ ), but was flush with the swept-back plate that separated the boundary-layer channel from the main duct. A scoop height of 0.13 inch was obtained when the ramp was flush with the body. Depressing the ramp into the body provided scoop heights up to 0.6 inch. The boundary-layer air was channeled to the sides and exhausted through gill-like outlet flaps. These gills could be opened and closed; unless otherwise noted, however, all data presented herein were obtained with the gills open. The total area of the six gills as viewed from the side was approximately 17 square inches. In open position, the gills made an angle of approximately  $14^\circ$  with the plane of symmetry. Photographs of the boundary-layer bleed system are shown in figure 3.

Details of the two inlets tested and the corresponding subsonic diffuser-area distributions are presented in figure 4. The  $25^\circ$  inlet, having a  $25^\circ$  cone half-angle, was so designed that the oblique shock would intersect the cowl lip at a Mach number of 2.0, when no body or control surface effects are assumed. The oblique shock of the  $30^\circ$  inlet was designed to fall ahead of the lip at a Mach number of 2.0, causing a resultant decrease in maximum mass-flow ratio of approximately 7 percent.

2747 Two force-measuring systems were used in this investigation. The first was an electrical strain-gage balance, consisting of two links mounted between the model and the support strut, calibrated to measure axial force and normal force in each link. The second system was the main-tunnel balance equipment to which the model support strut was connected external to the test section. This equipment was considered somewhat more reliable than the strain-gage balance and was used to measure gross lift and thrust-minus-drag. The support-strut drag tares were determined by a comparison between the two balance systems at zero angle of attack; this checked an earlier experimental determination of strut drag. Pitching moment about the reference center was determined with data from both balance systems.

The model support strut caused interference forces to act on the model. In the tests of the related model of reference 1, which was symmetrical about a horizontal plane and which utilized the same support system, a negative lift, probably due to the pressure field developed by the support strut acting on the top surface of the body and wing, was measured at zero angle of attack. To correct for this result, angle-of-attack shifts were made for the lift and drag data at each Mach number. For the asymmetrical configuration considered herein, it was not certain whether the same shifts would apply; therefore, no correction was made. The interference of the support strut on the zero-lift drag was estimated to be negligible because of the relatively small axial area projection of the affected region.

The model was also subject to interference from disturbances originating at the nose of the model and reflecting from the tunnel walls on to the wing tips and the tail pipe. Estimates of the strength and the location of these disturbances indicate that the effects were negligible at a free-stream Mach number of 2.0. At a free-stream Mach number of 1.5, the reflections cover a greater portion of the model and the exact magnitudes of the interference are uncertain, although it is believed that these magnitudes are small.

A sketch of the pressure instrumentation used in the investigation appears in figure 5. The survey equipment at station 50 was removed during most of the tests. Additional instrumentation consisting of total-pressure rakes mounted inside of and just aft of the cowl lip were installed for a portion of the tests to determine characteristics of the inlet flow. These rakes are visible in the photographs of figure 3.

The mass flow of air through the engine was controlled by an independently supported streamline plug which could be translated along the tail-pipe center line. The mass-flow ratio  $m/m_0$  was determined

by static-pressure measurements in the tail pipe (station 120), with the assumption that the flow was choked at the known minimum exit area. This technique has been shown to be reliable when the duct Mach number is reasonably low (on the order of 0.2). The pressure recovery and diffuser-exit Mach number were then computed from the mass flow and the static pressure measured at the diffuser exit (station 108).

The engine thrust was defined as the component in the free-stream direction of the term  $[mv_3 + (p_3 - p_0) A_3]$ , or total momentum, at station 120, minus the free-stream momentum of the main-duct mass flow  $mv_0$ . The internal lift of the engine was defined as the component normal to the free-stream direction of the total momentum at station 120. These forces were used to compute the external lift and drag of the configuration from the measured lift and thrust-minus-drag. The internal pitching moment of the engine, defined as the moment of the total momentum at station 120, was assumed to be zero for the present case because the moment reference center was on the tail-pipe center line.

## DISCUSSION

### External Forces and Moments

Lift, moment, and drag coefficients are presented for the 25°-inlet configuration as functions of angle of attack and control-surface deflection angle in figures 6 to 8. These data were obtained with supercritical inlet flow (maximum mass-flow ratio) and maximum boundary-layer-scoop height ( $h = 0.6$  in.). In addition to the curves presented for constant control-surface deflection angles, data are presented for the canard control aligned with the free stream ( $\delta_c = -\alpha$ , dashed lines). These data approximate the performance of the configuration with the control surface removed.

In figure 6, it may be observed that the lift coefficient is generally positive at  $\alpha = \delta_c = 0^\circ$ . This is in contrast to the data of reference 1, where negative lifts due to support-strut interference were measured with the same support system for a symmetrical model. It would be expected that interference lift for the present case would be in the same direction, if not of the same magnitude as that in reference 1, so that a positive lift apparently does exist at  $\alpha = \delta_c = 0^\circ$ , possibly because of the forebody shape. If it were assumed that the angle-of-attack shifts of reference 1, which varied from  $0.7^\circ$  at  $M_0 = 1.5$  to  $0.3^\circ$  at  $M_0 = 2.0$ , were valid for the present tests, the

angle of zero lift for  $\delta_c = 0^\circ$  would be approximately  $-0.7^\circ$  for all Mach numbers tested.

The pitching-moment data (fig. 7) indicate that the model was stable about the reference moment center for all conditions tested. It was possible to trim the model at all test angles of attack with the test range of control deflection angles.

Lift-drag ratios obtained from the faired data of figures 6 and 8 are presented in figure 9. For  $\delta_c = 0^\circ$ , maximum lift-drag ratios in excess of 5 were measured at all test Mach numbers. Deflection of the control surface from  $0^\circ$  to  $5^\circ$ , or more, decreased the maximum lift-drag ratios. Contrary to the usual variation at supersonic speeds, the maximum lift-drag ratios apparently increase slightly with an increase of Mach number at positive angles of attack. This is probably an effect of support-strut interference; it has been estimated that at the lower Mach numbers the magnitude of the lift-drag ratios would be somewhat higher at positive angles and lower at negative angles.

The variations of drag coefficient with inlet mass-flow ratio and boundary-layer-scoop height are presented in figures 10 to 12 for the  $25^\circ$ -inlet configuration. A decrease in mass-flow ratio causes an appreciable increase in drag; the additive drag resulting from the thrust definition is primarily responsible. An increase in boundary-layer-scoop height  $h$  causes an appreciable drag increase at all conditions. The increment of supercritical drag coefficient ranges from approximately 0.001 to more than 0.005 as  $h$  is increased from 0 to 0.6 inch.

The data presented in figures 10 to 12 were obtained with the boundary-layer-outlet gills open. When the boundary-layer-scoop height was zero, closing the gills resulted in a drag coefficient decrease of approximately 0.0015 for all Mach numbers. At  $M_0 = 2.0$ , the minimum drag coefficient of the configuration at  $\alpha = 0^\circ$  and  $h = 0$  would then be approximately 0.020 with the gills closed. No attempt was made to optimize the amount of gill opening at boundary-layer-scoop heights other than zero.

The drag coefficient of the  $30^\circ$ -inlet configuration was approximately the same as for the  $25^\circ$  inlet at a given mass-flow ratio. However, the supercritical drag coefficient was higher for the  $30^\circ$  inlet because of the higher lip angle and the mass-flow spillage associated with the oblique shock position.



Lift and moment coefficients for the  $25^\circ$ -inlet configuration are presented as functions of mass-flow ratio and scoop height in figure 13 for a Mach number of 2.0. The effects on lift are very slight, and the variations of moment are small compared with the effects of angle of attack and control-surface deflection angle (fig. 7). Data obtained with the  $30^\circ$  inlet and for other Mach numbers were similar.

The effects of inlet mass-flow ratio and boundary-layer-scoop height on lift-drag ratio are shown in figure 14(a) for a Mach number of 2.0. For a boundary-layer-scoop height of 0.6 inch, a reduction in mass-flow ratio of 0.10 from the supercritical value reduces the maximum lift-drag ratio from approximately 5.3 to 5.0. A decrease in the scoop height to zero ( $h = 0$ ) increased the maximum lift-drag ratio for supercritical flow to 5.5 with the gills in the open position. Closing the gills resulted in an additional increase to approximately 5.7.

A comparison of the lift-drag ratios measured with the two inlets tested is shown in figure 14(b) for supercritical inlet flow and a scoop height of 0.6 inch. The  $30^\circ$ -inlet configuration had a maximum lift-drag ratio of approximately 5.0 compared with 5.3 for the  $25^\circ$  inlet.

#### Flow Survey Ahead of Inlet

The Mach number measured with the wedge mounted at station 50 is shown in figure 15 for  $M_0 = 2.0$  as a function of angle of attack, control-surface deflection, and boundary-layer-scoop height. This inlet Mach number, determined by the measured pressures and two-dimensional flow theory, presumably is valid only at the point of measurement. It should, however, be representative of the flow field that enters the inlet.

The effect of angle of attack (fig. 15(a)) is relatively significant; an increase from  $\alpha = 0^\circ$  to  $\alpha = +10^\circ$  causes a reduction in Mach number of more than 0.1. Deflection of the canard control surface, on the other hand, has but a small effect on the Mach number.

An increase in boundary-layer-scoop height (fig. 15(b)) causes a small increase in the inlet Mach number, as would be expected from consideration of the change in flow direction associated with the ramp movement. This Mach number change should not affect the inlet performance appreciably; for the complete range of ramp movement, the resulting change in inlet shock losses is of the order of only 1 percent.

The results of the boundary-layer survey at station 50 are presented as contour plots of indicated total pressure divided by free-stream total pressure in figures 16 to 18 for a Mach number of 2.0. Although sharp-nosed static-pressure probes were included in the instrumentation, they were not considered reliable for variable-angle-of-attack, supersonic flow; therefore, no attempt was made to correct the total pressures for shock losses. The dashed lines in the drawings represent the location of the inlet and of the plate separating the main duct and the boundary-layer duct. The vertical scales indicate the distance in inches from the ramp surface at the position of the rakes.

The effect of boundary-layer-scoop height  $h$  at  $\alpha = 0^\circ$  and  $\delta_c = 0^\circ$  is shown in figure 16. An increase in  $h$  apparently increases the thickness of the boundary layer somewhat, but decreases significantly the amount of boundary layer that enters the inlet. At  $h = 0.6$  inch, there is an effect in the corner of the ramp that is believed to be a vortex caused by air spilling over the diverging walls of the ramp. In this respect, the flow is similar to that described in reference 3 for a flush-type inlet at subsonic speeds.

The effects of angle of attack are shown in figure 17 for scoop heights of 0.13 (ramp flush with body) and 0.6 inch. The canard control surface was aligned with the free stream for these cases in an attempt to isolate the effect of the body. As  $\alpha$  is increased from  $0^\circ$  to  $10^\circ$ , there is a marked tendency for the thickness of the boundary layer to decrease. This tendency was observed previously for the lower surfaces of bodies of revolution at angle of attack in references 4 and 5. At negative angles, the boundary-layer thickness increases. At  $\alpha = -7^\circ$  the thickness is roughly twice that at  $\alpha = 0^\circ$ . An additional disturbance was observed at  $\alpha = -7^\circ$  for the outermost rake (fig. 17(a)). This disturbance probably was a part of the vortex due to separation of the cross flow about the body, an effect similar to those observed for a body of revolution in reference 4.

At  $\alpha = 10^\circ$ , no ramp vortex was observed for  $h = 0.6$  inch (fig. 17(b)). This probably is due to the divergence of the flow on the underside of a body at angle of attack; if the streamlines are parallel with the diverging ramp walls, there will be no tendency for a vortex to form.

The indicated total pressures at a distance from the body were also observed to be a function of the angle of attack. This effect corresponds to the changes in Mach number shown in figure 15 and the resultant changes in shock losses.

The effects of control-surface deflection on the flow are shown in figure 18 for  $h = 0.13$  inch and  $\alpha = -7^\circ, 0^\circ$ , and  $10^\circ$ . At  $\alpha = 0^\circ$ , the thickness of the boundary layer is greater at  $\delta_c = 10^\circ$  than at  $\delta_c = -10^\circ$ . A disturbance resembling cross-flow separation may also be seen at  $\delta_c = 10^\circ$ . The downwash from the control surface presumably is responsible for these two effects. Similar effects for a body of revolution combined with a canard control surface are presented in reference 5.

At  $\alpha = 10^\circ$ , a significant difference between the flows for  $\delta_c = -10^\circ$  and  $10^\circ$  exists. The pressure gradient observed at a considerable distance from the body for  $\delta_c = 10^\circ$  is probably due to a strong shock caused by the canard control. The lower surface of the control at the leading edge makes an angle of approximately  $26^\circ$  with the free stream for this condition,  $3^\circ$  greater than the limiting angle for shock attachment at a Mach number of 2.0.

At  $\alpha = -7^\circ$ , the plot for  $\delta_c = 7^\circ$  shows the cross-flow-separation effect. At  $\delta_c = -10^\circ$ , the upwash due to the negative lift of the control is opposed to the main cross flow of air about the body and a distorted pattern results.

#### Diffuser Performance

Diffuser pressure recovery is plotted as a function of mass-flow ratio, boundary-layer-scoop height and angle of attack in figure 19 for the  $25^\circ$ -inlet configuration and in figure 20 for the  $30^\circ$ -inlet configuration. Also presented are lines of constant diffuser-exit Mach number  $M_2$ . Flagged symbols and dashed lines indicate unstable inlet operation or pulsing. A dashed line shown with no flagged symbol attached indicates that the limit of stable operation was reached, but that no data were obtained under pulsing conditions. The slope of the dashed lines in these cases is arbitrary and does not necessarily correspond to the amplitude of the pulsations.

An increase in boundary-layer-scoop height at low angles of attack generally resulted in an increased maximum pressure recovery. One exception to this appears in figure 19(c) for  $\alpha = 0^\circ$ . Here an increase from  $h = 0.4$  to  $0.6$  inch resulted in a maximum pressure-recovery decrease of 0.04. This effect is similar to the effect reported for a related inlet in reference 6 in which it was found that higher pressure recoveries could be attained when some boundary layer was allowed to enter the inlet than when all the boundary layer was removed. At high

angles of attack, the effect of scoop height usually was small; while at negative angles, the effect was very significant. This corresponds to the variation of boundary-layer thickness with angle of attack (fig. 17).

At high angles of attack and low Mach numbers for the  $30^\circ$  inlet, the pressure recovery for  $h = 0$  was higher than that for  $h = 0.6$  inch. When the boundary layer was allowed to enter the inlet at these conditions, the static-pressure rise associated with the subcritical operation of the inlet induced flow separation ahead of the cone. This flow separation caused a two-shock configuration to replace the single shock from the cone tip and a resultant decrease in shock losses was realized. When the boundary layer was bled off at  $h = 0.6$  inch, this favorable separation phenomenon did not occur.

In general, the diffuser pressure recoveries showed a tendency to increase as  $\alpha$  was increased from  $0^\circ$  to  $10^\circ$ . The decrease of inlet Mach number at high angles of attack (fig. 15) undoubtedly is an important factor in this effect, as well as the variation of boundary-layer thickness. At negative angles of attack, the recoveries were relatively low.

For a Mach number of 2.0, the pressure recoveries measured for the  $30^\circ$  inlet were generally higher than those for the  $25^\circ$  inlet. At  $\alpha = 0^\circ$ , the maximum recoveries were 0.83 and 0.79 for the two inlets, respectively. There were several design differences between the two inlets: cone angle, oblique shock position, lip angle, diffuser area distribution, local curvatures, and so forth. It is believed that the cone angle was one of the important differences. For the  $25^\circ$  inlet at  $M_0 = 2.0$ , a separated region on the cone surface, apparently the result of the interaction of the normal shock with the cone boundary layer, was observed in schlieren photographs. Data obtained with the inlet rakes also showed this separated region. For the  $30^\circ$  inlet, the Mach number behind the oblique shock was lower than that for the  $25^\circ$  inlet, and therefore the static-pressure rise across the normal shock was less. Separation of this type was not observed for the  $30^\circ$  inlet, and it is believed that this fact is partially responsible for the higher pressure recoveries.

The stable operating range of both inlets was greatly affected by scoop height, angle of attack, and Mach number. There would appear to be no simple formula for predicting the stability characteristics of these inlets. The characteristics may, of course, be a function of the particular boundary-layer-removal system employed as well as of the inlet design.

The effect of canard control-surface deflection on the diffuser performance is shown in figure 21 for the  $25^\circ$  inlet at  $\alpha = 0^\circ$ .

Data are presented for  $M_0 = 1.5$  and  $2.0$  and for  $h = 0$  and  $0.6$  inch.

In general, a positive deflection impaired the performance, while a negative deflection improved it. Although data were not obtained at all angles of attack, the data available and the results of the boundary-layer survey ahead of the inlet (fig. 18) indicate that the effect is similar throughout the angle-of-attack range.

Data obtained with the total-pressure rakes at the diffuser exit for  $M_0 = 2.0$  are presented in figures 22 and 23 as contour plots of total pressure divided by free-stream total pressure. The static pressures, which were essentially constant across the diffuser-exit station, are also indicated for reference. These data correspond to the diffuser characteristics shown in figures 19 and 20.

Figure 22 indicates the effect of mass-flow ratio and boundary-layer-scoop height for the  $25^\circ$ -inlet configuration at  $\alpha = 0^\circ$ . Both of these parameters affect the gradients and range of total pressure (indicated by the number and spacing of the contour lines) and the location of the maximum pressure. The mass-flow ratio (and the corresponding diffuser-exit Mach number) apparently has the greater effect on the pressure gradients.

Typical effects of angle of attack on the flow for the  $25^\circ$ - and  $30^\circ$ -inlet configurations are shown in figure 23 for  $h = 0.6$  inch. Test points selected were the maximum-pressure-recovery points at each angle of attack. For the  $25^\circ$  inlet, the location of the maximum total pressure shifts upward, as might be expected, as  $\alpha$  is increased from  $0^\circ$  to  $10^\circ$ . For the  $30^\circ$  inlet, however, a downward shift occurs for the same conditions. In each case the pressure gradients are reduced at  $\alpha = 10^\circ$ . At  $\alpha = -6.9^\circ$ , the flow patterns are essentially the same as at  $\alpha = 0^\circ$ .

No region of separated flow was observed at the diffuser exit for either of the inlet configurations. This is in contrast to reference 6, where separated regions were detected for a scoop inlet similar to the  $25^\circ$  inlet of the present investigation. The Reynolds number, which was approximately 4.5 times as large for the present investigation as for reference 6 when based on corresponding dimensions, may be one of the factors responsible for this effect.

#### SUMMARY OF RESULTS

An experimental investigation of a canard-type missile configuration with an underslung scoop inlet was conducted in the Lewis 8- by 6-foot supersonic wind tunnel at Mach numbers from 1.5 to 2.0 for a

range of angles of attack, control-surface deflection angles, boundary-layer-scoop heights, and inlet mass-flow ratios. Two inlets were tested, and total-pressure surveys were made ahead of the inlet and at the diffuser exit. The Reynolds number of the investigation was approximately  $8.4 \times 10^6$  based on the mean aerodynamic chord of the wing. The following results were obtained:

1. Lift-drag ratios in excess of 5 were measured at all test Mach numbers.

2. An increase in boundary-layer-scoop height or a decrease in inlet mass-flow ratio caused significant increases in drag coefficient but had no appreciable effect on lift or pitching moment.

3. At a Mach number of 2.0, the  $30^\circ$ -inlet configuration had a maximum pressure recovery of 0.83 at zero angle of attack, compared with 0.79 for the  $25^\circ$  inlet.

4. Diffuser pressure recoveries tended to improve as the angle of attack increased from  $0^\circ$  to  $10^\circ$  because of favorable effects on boundary-layer-thickness and inlet Mach number. Recoveries at negative angles of attack were generally poor. The effect of boundary-layer-scoop height was much more pronounced at negative angles than at positive angles because of the variation of boundary-layer thickness.

5. Positive canard control-surface deflections decreased maximum pressure recoveries and negative deflections tended to increase the pressure recoveries, corresponding to boundary-layer changes induced by the downwash from the surface.

Lewis Flight Propulsion Laboratory  
National Advisory Committee for Aeronautics  
Cleveland, Ohio

## REFERENCES

1. Obery, Leonard J., and Krasnow, Howard S.: Performance Characteristics of Canard-Type Missile with Vertically Mounted Nacelle Engines at Mach numbers 1.5 to 2.0. NACA RM E52H08, 1952.
2. Kremzier, Emil J., and Davids, Joseph: Performance Characteristics of Canard-Type Missile with Wing-Mounted Nacelle Engines at Mach Numbers 1.5 to 2.0. NACA RM E52J08, 1952.
3. Sacks, Alvin H., and Spreiter, John R.: Theoretical Investigation of Submerged Inlets at Low Speeds. NACA TN 2323, 1951.
4. Luidens, Roger W., and Simon, Paul C.: Aerodynamic Characteristics of NACA RM-10 Missile in 8- by 6-Foot Supersonic Wind Tunnel at Mach Numbers from 1.49 to 1.98. I - Presentation and Analysis of Pressure Measurements (Stabilizing Fins Removed). NACA RM E50D10, 1950.
5. Fradenburgh, Evan A., Obery, Leonard J., and Mello, John F.: Influence of Fuselage and Canard-Type Control Surface on the Flow Field Adjacent to a Rearward Fuselage Station at a Mach Number of 2.0 - Data Presentation. NACA RM E51K05, 1952.
6. Goelzer, H. Fred, and Cortright, Edgar M., Jr.: Investigation at Mach Number 1.88 of Half of a Conical-Spike Diffuser Mounted as a Side Inlet with Boundary-Layer Control. NACA RM E51G06, 1951.

2747

TABLE I - GEOMETRIC CHARACTERISTICS OF BODY-ENGINE

(All dimensions in inches.)

## (a) Forebody

Equation for cross-sectional shape:

$$\frac{x}{4.5} = \pm \sqrt{1 - \left(\frac{y}{9}\right)^2 - K\left(\frac{9}{y}\right)}$$

## (b) Afterbody

[External: Semi-elliptical cross-section; minor axis horizontal, on reference line ahead of station 70, on engine center line behind station 70; minor diam. 9.00; major diam.  $2H_1$ .  
Internal: Semi-elliptical cross-section; major axis horizontal on engine center line; major diam. 8.81; minor diam.  $2H_2$ .]

## (c) Engine center line

$y_e$  is height of center line above reference line

Model station	K
0	0.3849
6	.3381
12	.2671
18	.1950
24	.1312
30	.0796
36	.0426
42	.0184
48	.00555
54	.00070
60	0

Model station	$H_1$	$H_2$
60	9.00	0
66	8.90	0
72	8.55	0
78	7.90	.32
84	7.07	1.35
90	6.20	2.48
96	5.33	3.60
103	4.50	4.41

Model station	$y_e$
55.75	-0.13
60	-.13
66	-.08
72	.06
78	.27
84	.57
90	.89
96	1.20
103-138	1.50

## (d) Diffuser shell

[Semi-circular about engine center line.]

Model station	25° Inlet		30° Inlet	
	Outside radius	Inside radius	Outside radius	Inside radius
55.75	3.89	3.89	3.89	3.89
56	3.95	3.91	4.00	3.94
57	4.10	4.03	4.25	4.16
58	4.24	4.15	4.32	4.23
60	4.42	4.33	4.42	4.33
63-103	4.50	4.41	4.50	4.41

## (e) Centerbody

[Semi-circular cross-section. Axis on upper diffuser surface.]

Model station	25° Inlet radius	30° Inlet radius
51.58	0	----
51.95	0.17	0
55	1.59	1.76
56	1.99	2.34
57	2.14	2.80
58	2.25	2.92
60	2.38	3.00
66	1.83	2.68
72	1.00	1.83
79	0	0.26
80	----	0



CONFIDENTIAL

NACA RM ES2J22

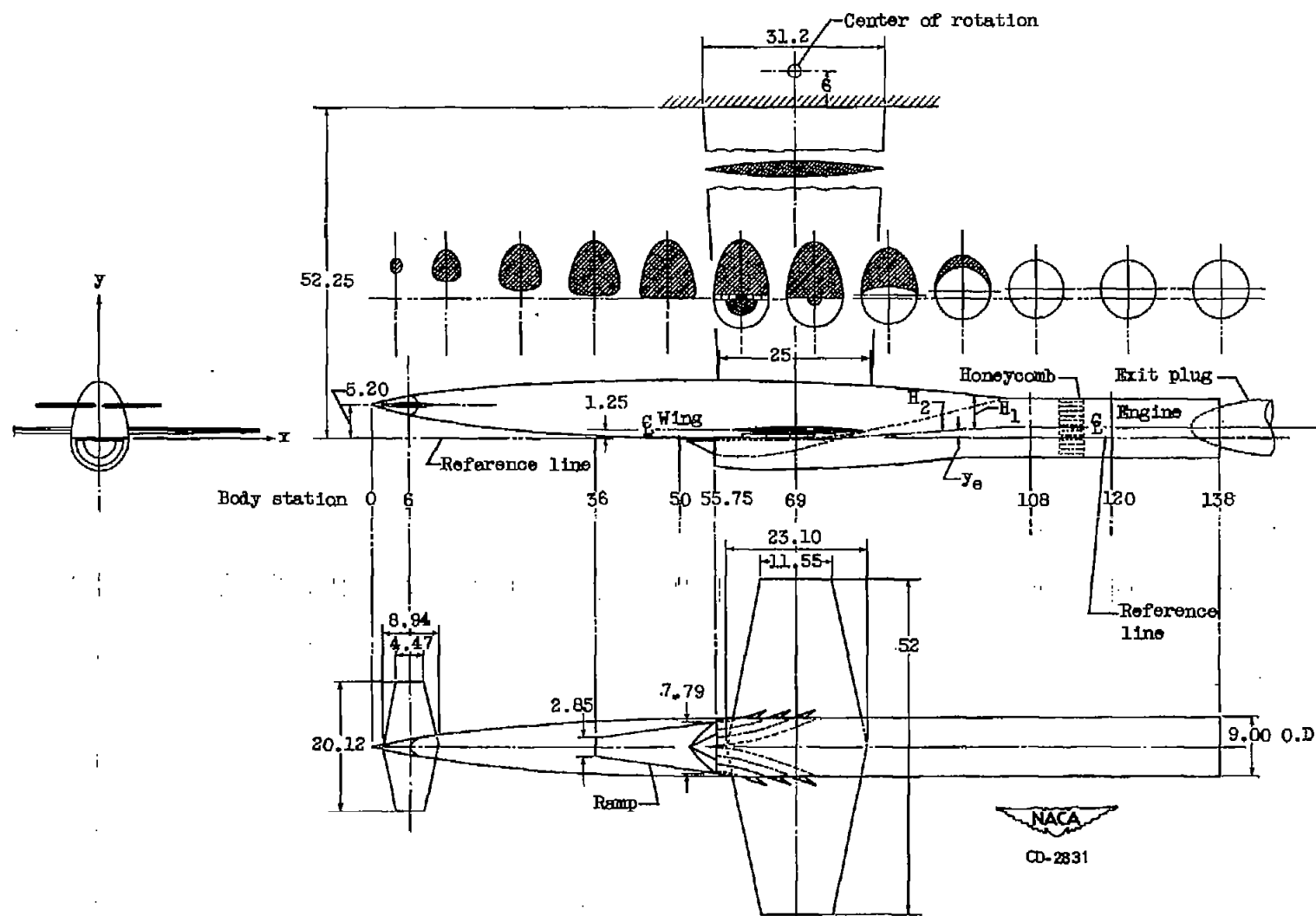


Figure 1. - Sketch of model and support strut. (All dimensions in inches.)

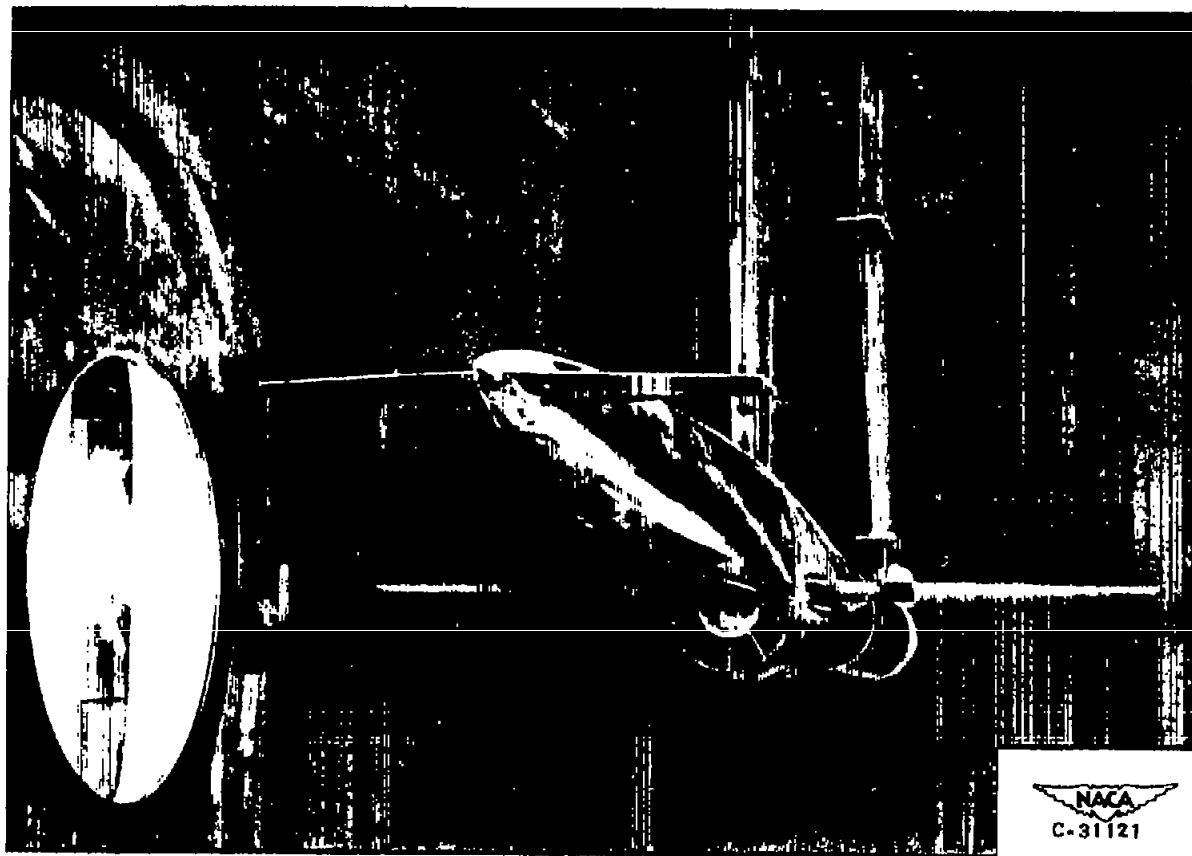
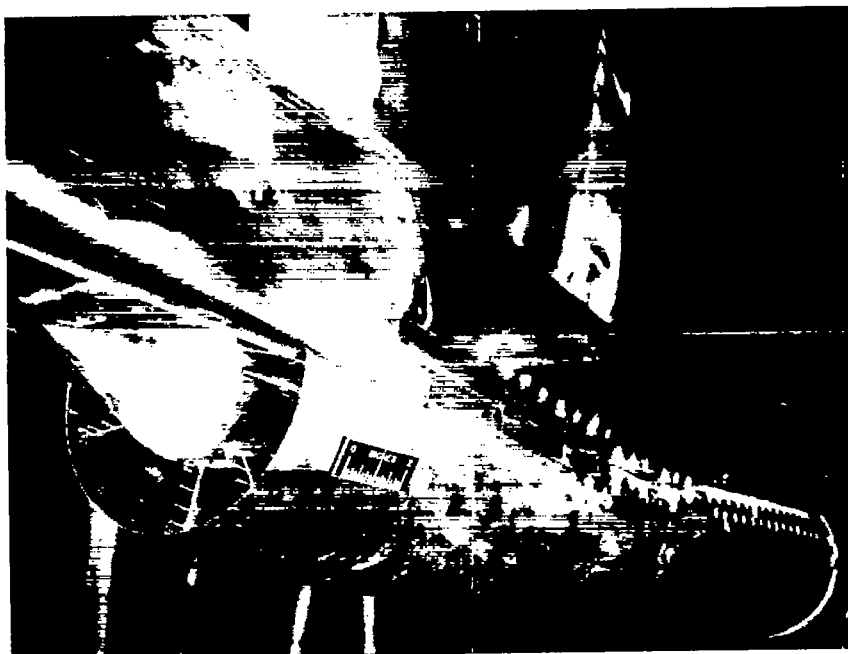
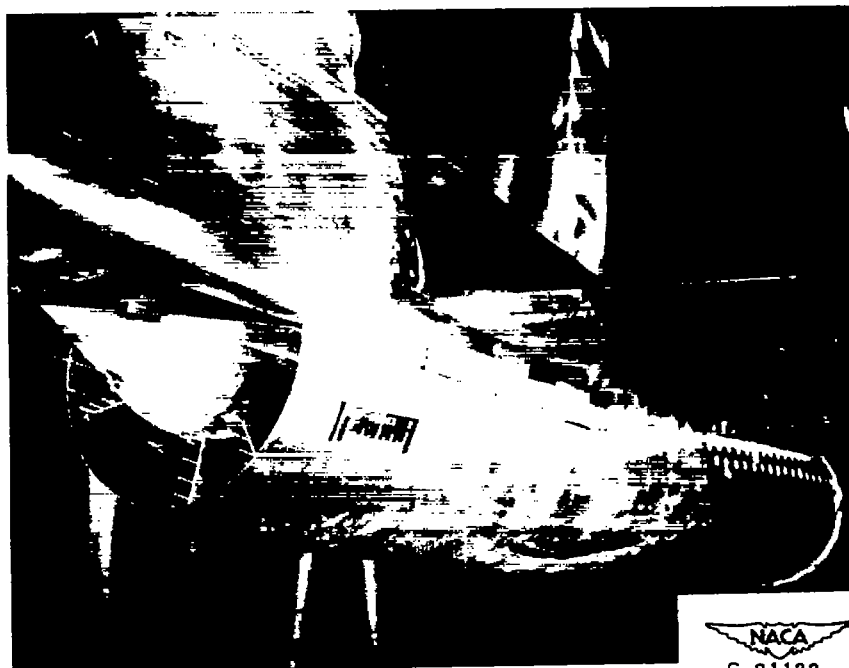


Figure 2. - Model installed in 8- by 6-foot supersonic wind tunnel.



(a) Boundary-layer-scoop height, 0 inch. Gills closed.



(b) Boundary-layer-scoop height, 0.6 inch. Gills open.

Figure 3. - Details of boundary-layer bleed system.

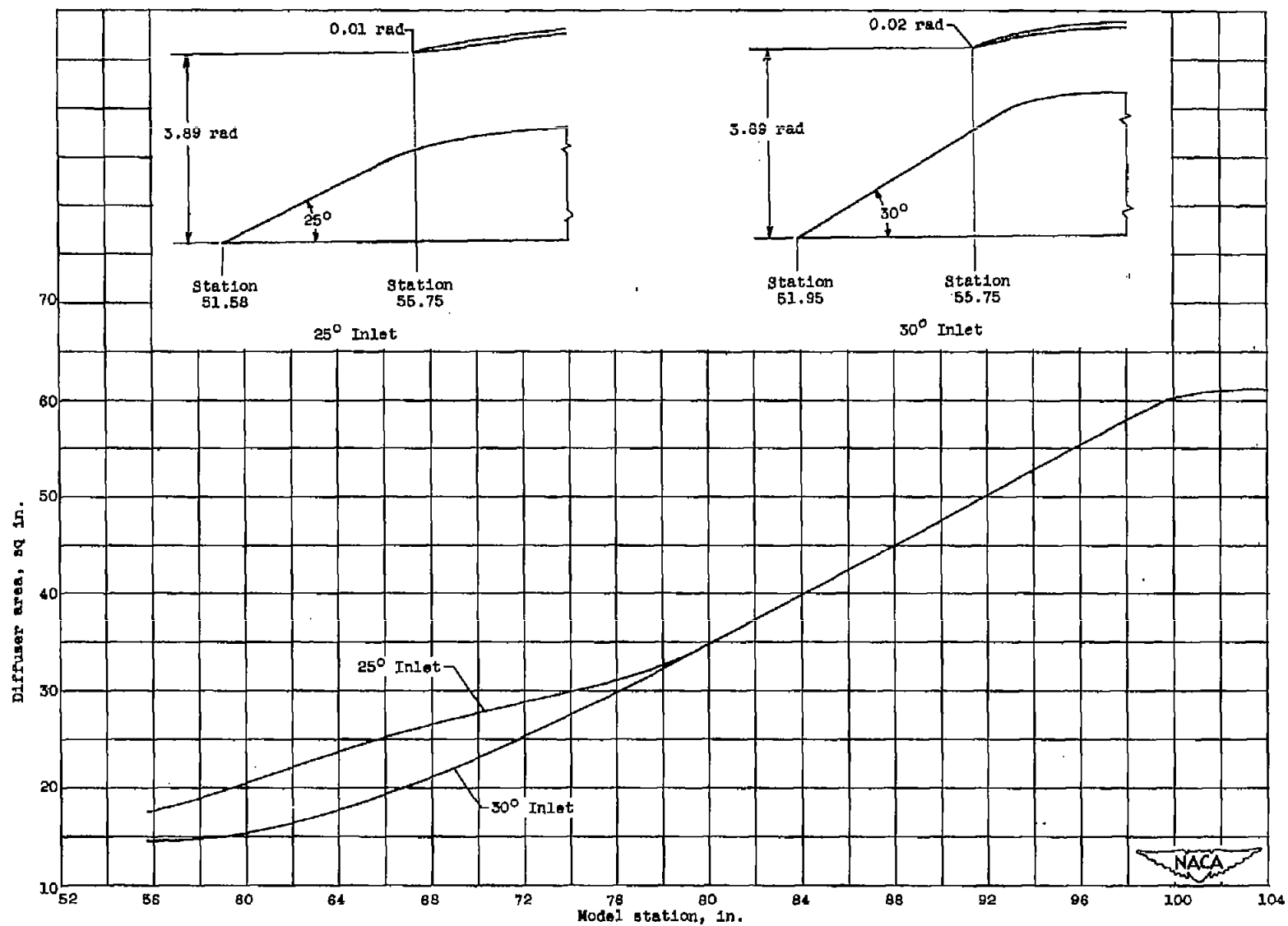
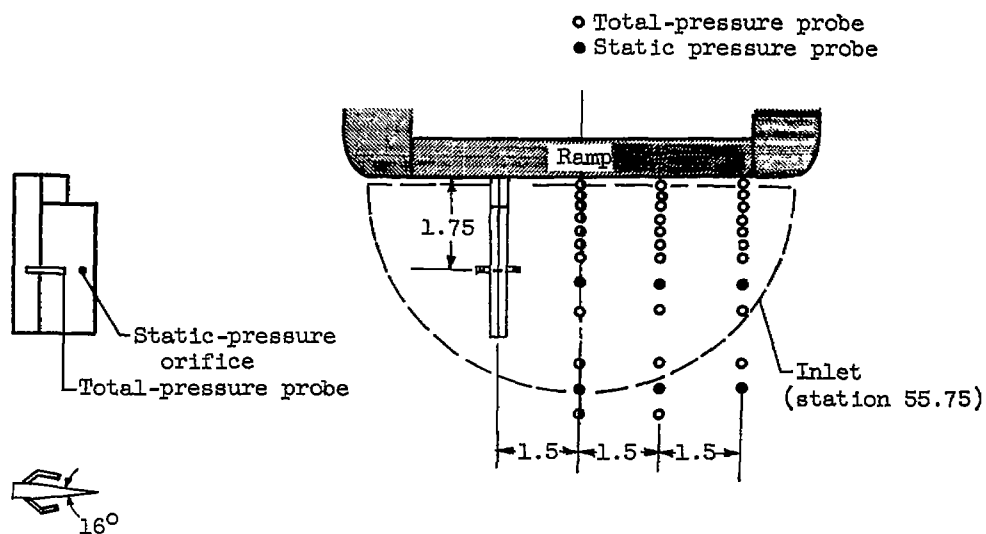
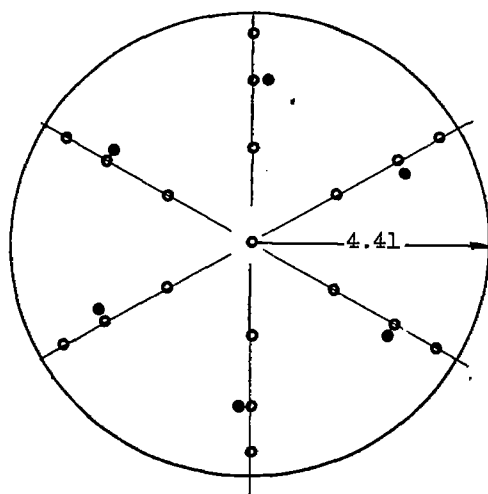


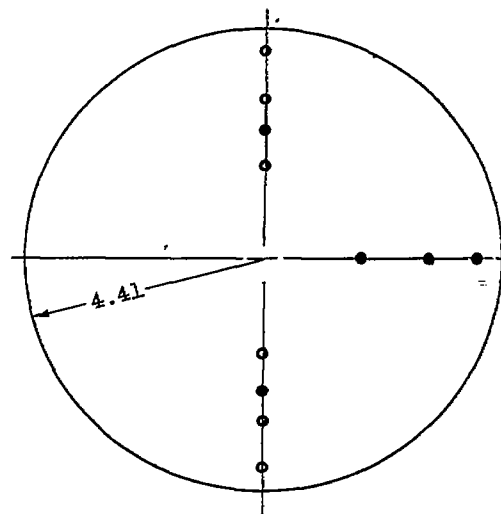
Figure 4. - Inlet details and corresponding diffuser-area distributions.



(a) Station 50. Wedge (three views) and boundary-layer rakes.



(b) Station 108.



(c) Station 120.

Figure 5. - Pressure instrumentation. (All dimensions in inches.)

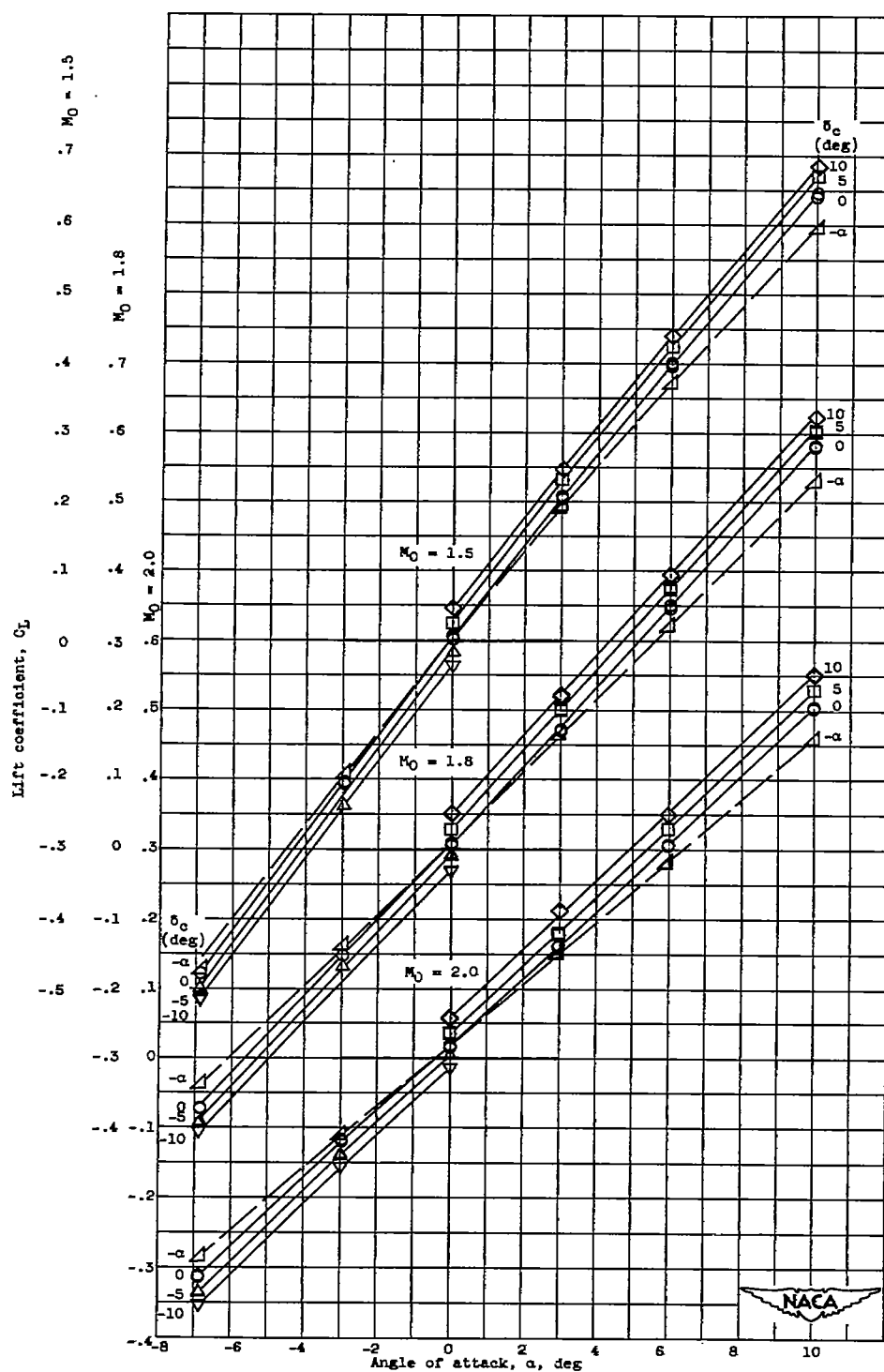


Figure 6. - Variation of lift coefficient with angle of attack for  $25^\circ$ -inlet configuration at several free-stream Mach numbers and canard control-surface deflection angles for supercritical inlet flow. Boundary-layer-scoop height, 0.6 inch.

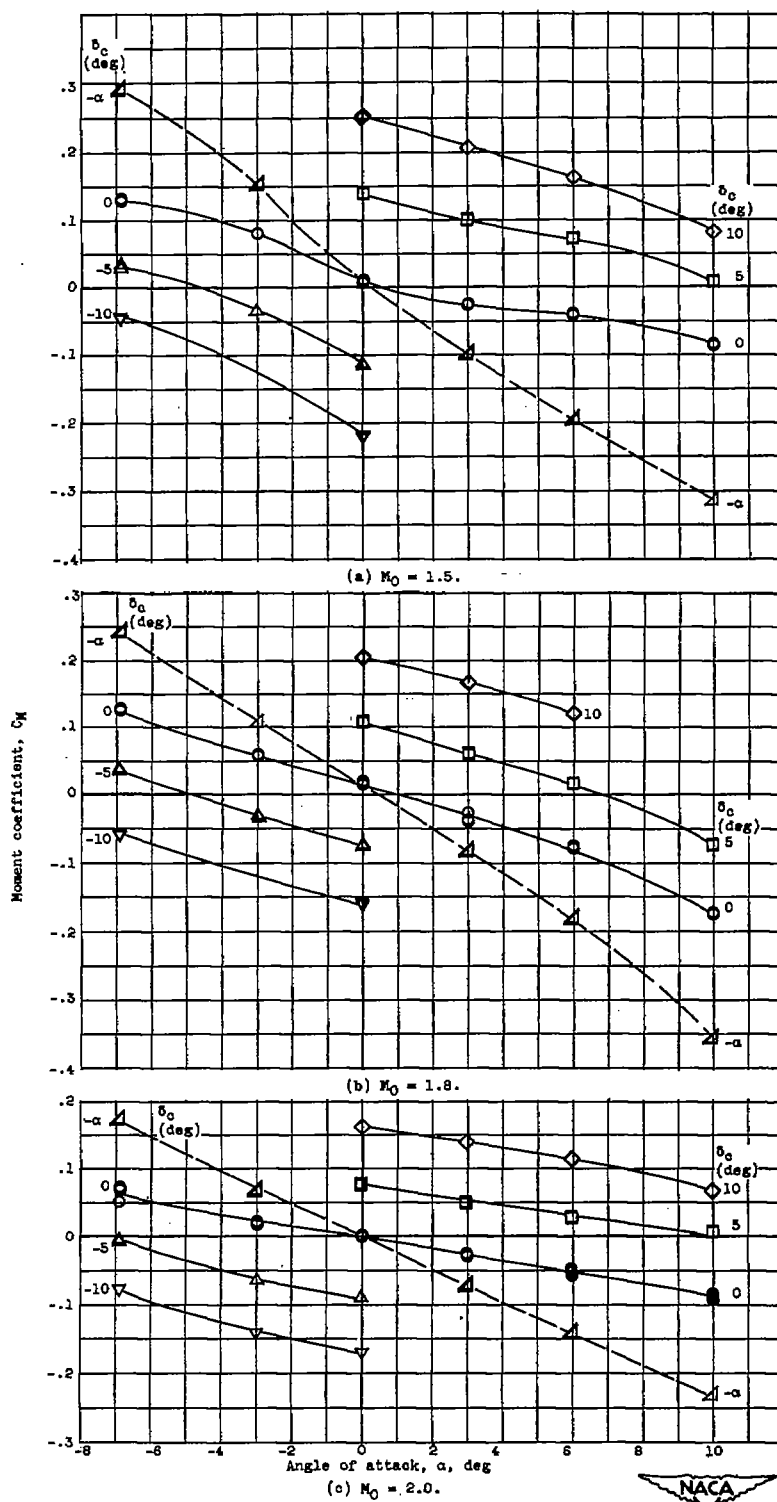


Figure 7. - Variation of moment coefficient with angle of attack for 25°-inlet configuration at several free-stream Mach numbers and capard control-surface deflection angles for supersonic inlet flow. Boundary-layer-scoop height, 0.6 inch.

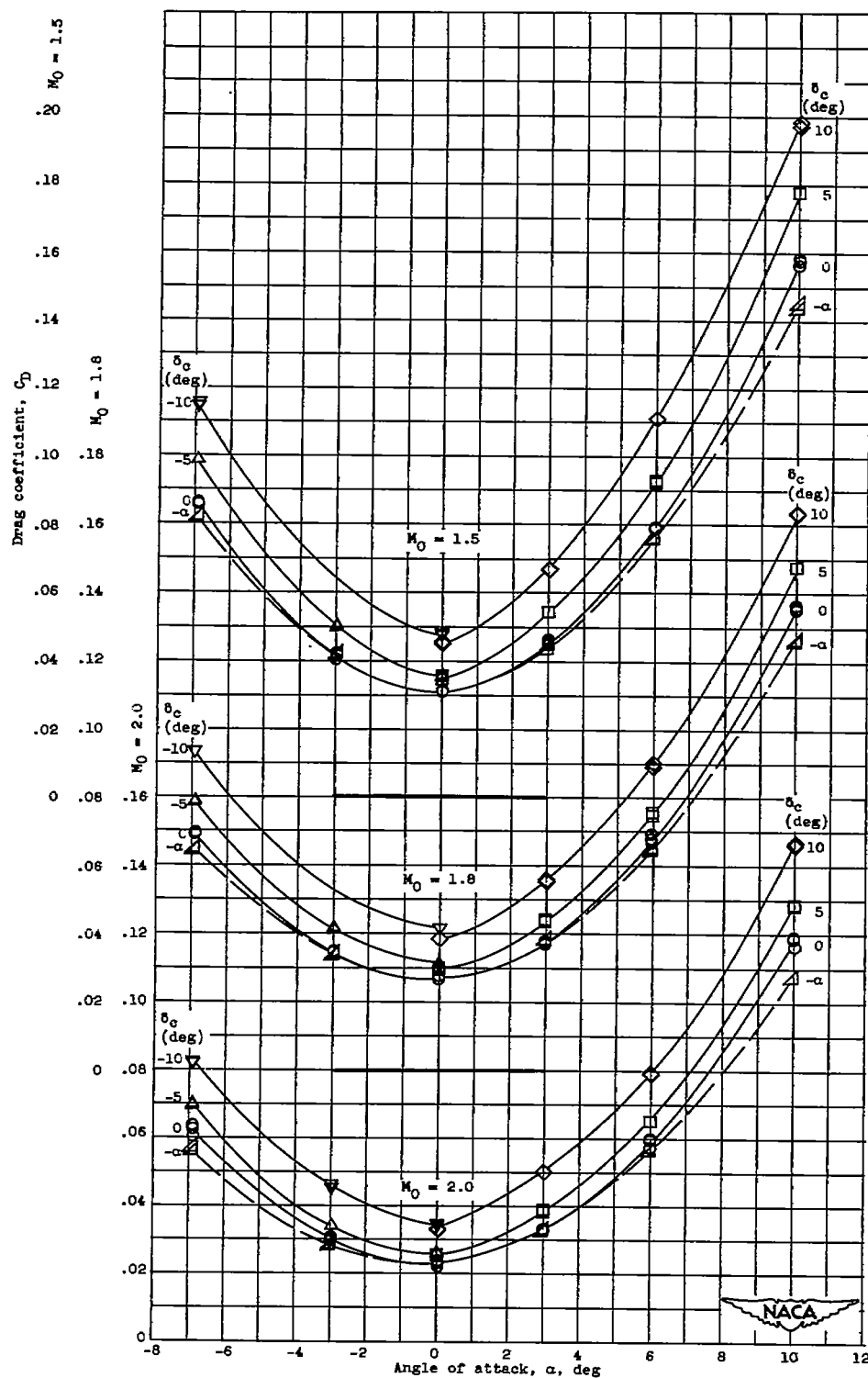


Figure 8. - Variation of drag coefficient with angle of attack for 25°-inlet configuration at several free-stream Mach numbers and canard control-surface deflection angles for supercritical inlet flow. Boundary-layer-scoop height, 0.8 inch.



CONFIDENTIAL

NACA RM E52J22

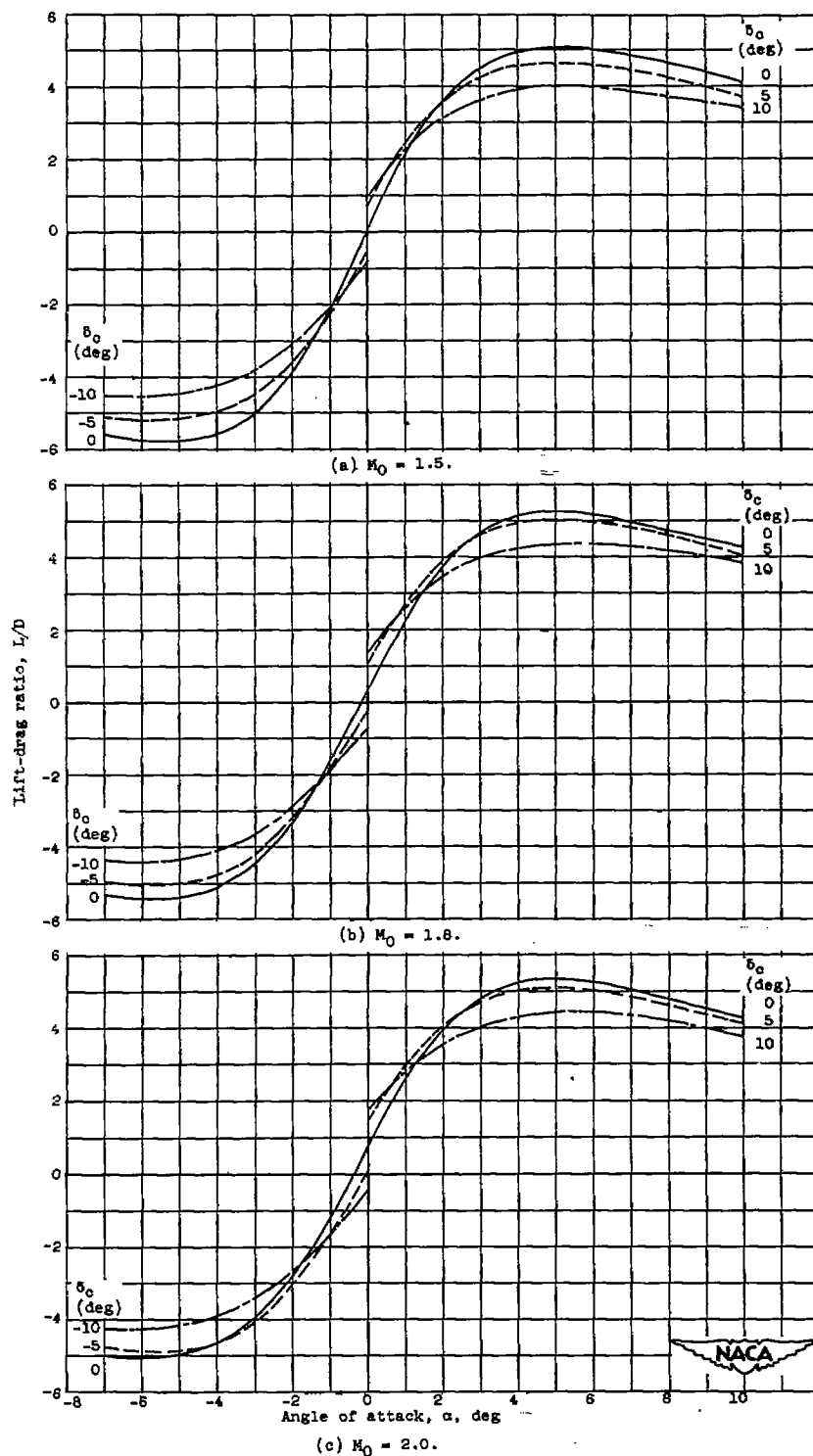


Figure 9. - Variation of lift-drag ratio with angle of attack for 25°-inlet configuration at several free-stream Mach numbers and canard control-surface deflection angles for supercritical inlet flow. Boundary-layer-scoop height, 0.6 inch.

CONFIDENTIAL

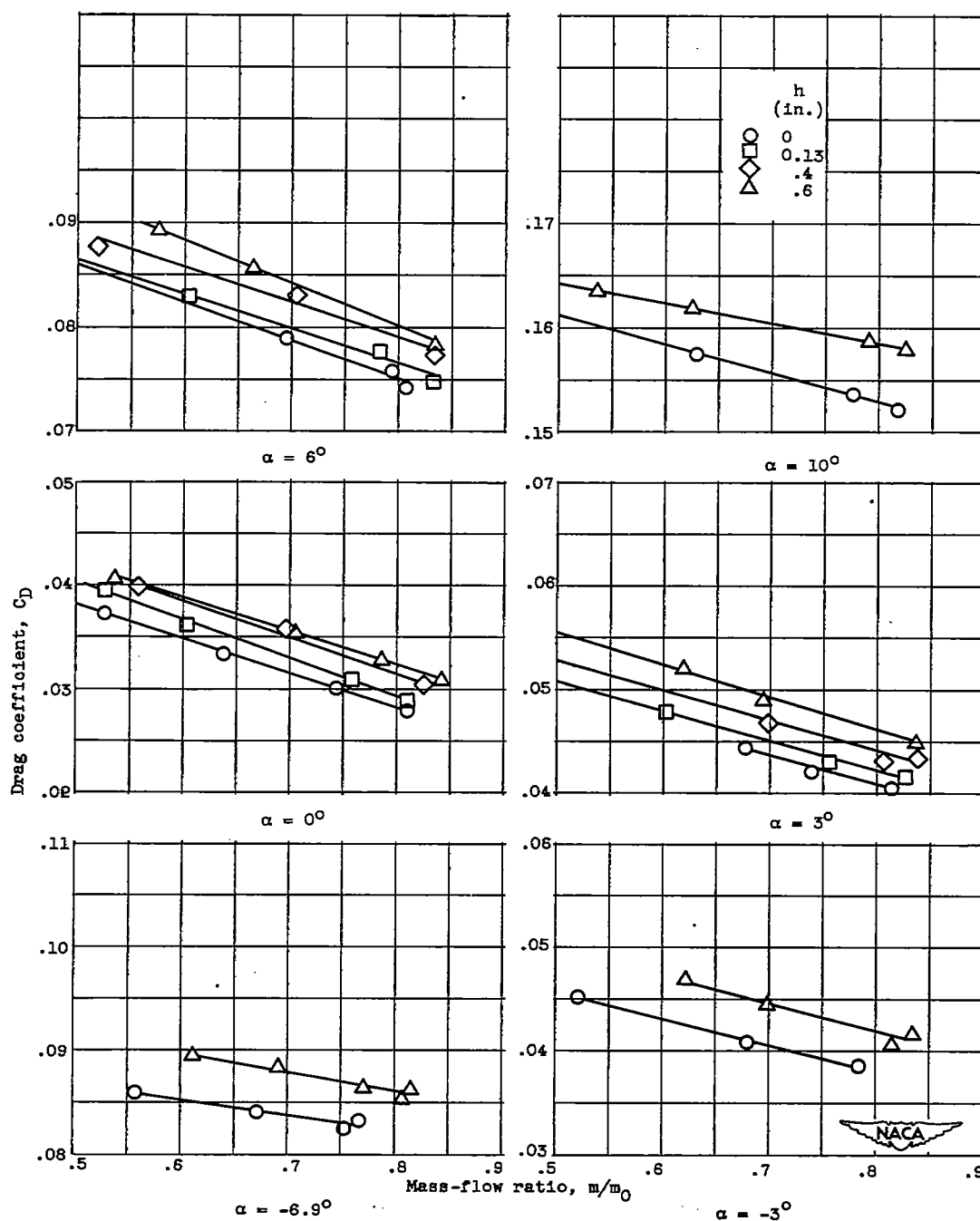


Figure 10. - Variation of drag coefficient with inlet mass-flow ratio and boundary-layer-scoop height for 25°-inlet configuration. Free-stream Mach number, 1.5; canard control-surface deflection angle, 0°.

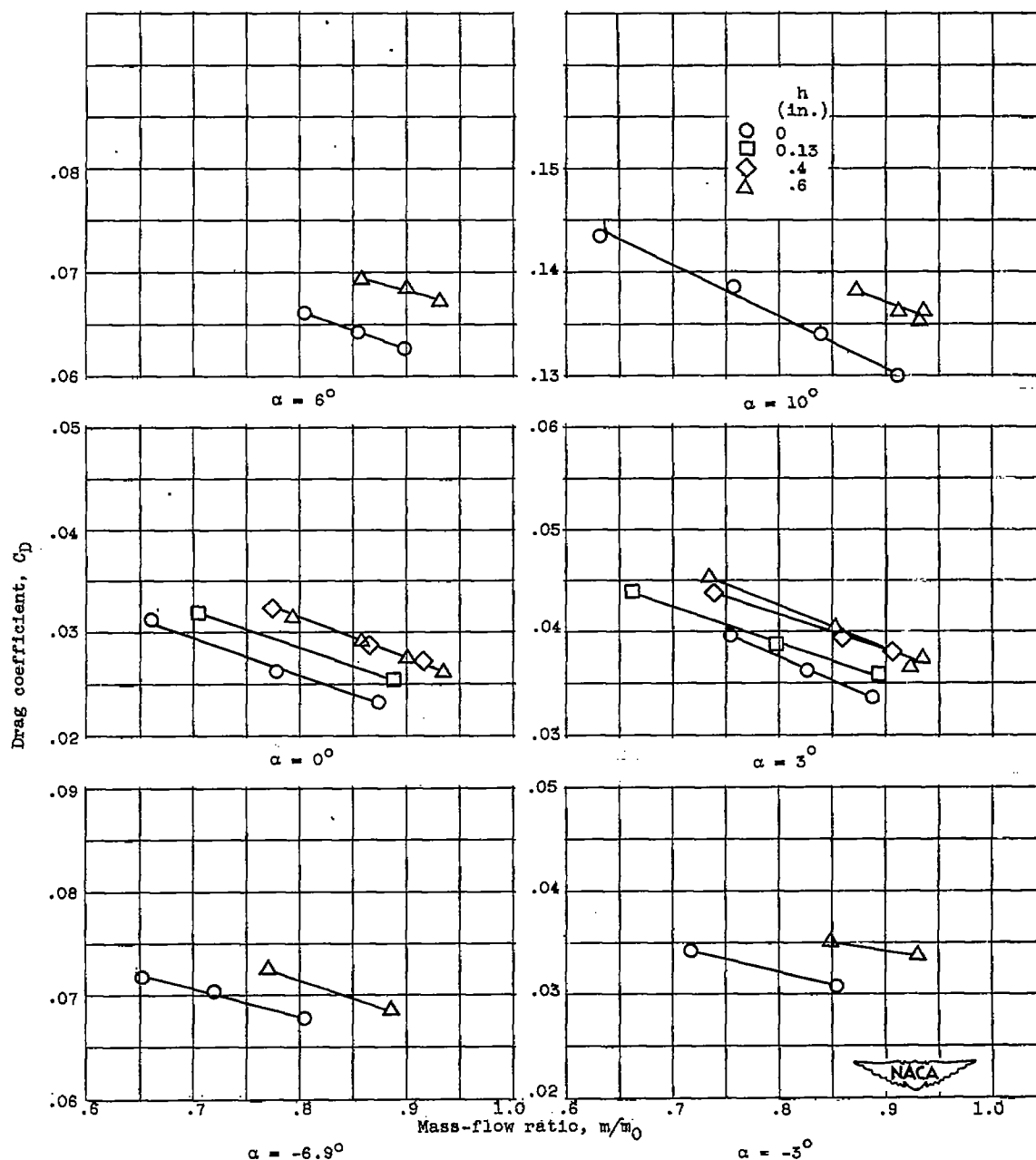


Figure 11. - Variation of drag coefficient with inlet mass-flow ratio and boundary-layer-scoop height for 25°-inlet configuration. Free-stream Mach number, 1.8; canard control-surface deflection angle, 0°.

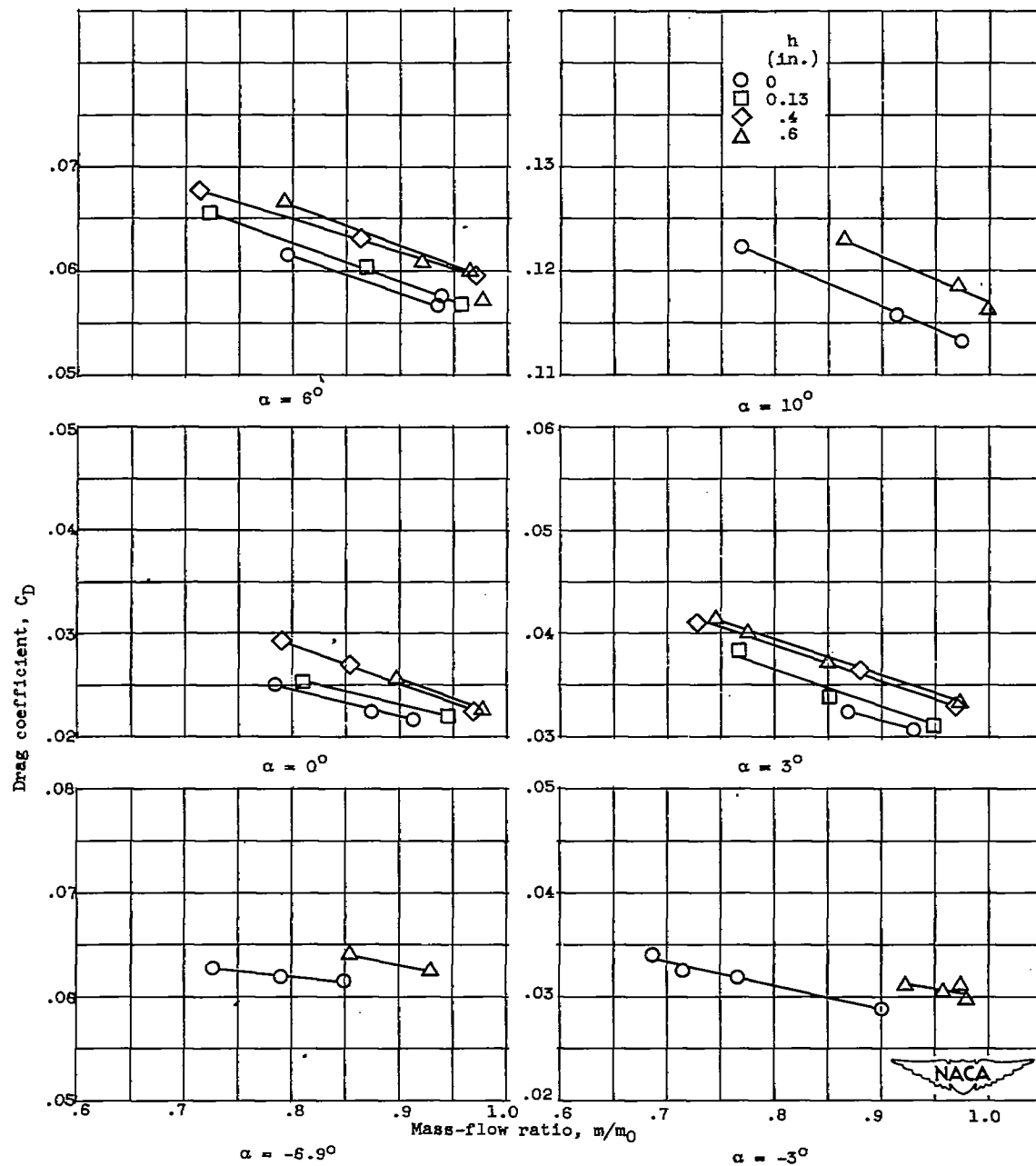


Figure 12. - Variation of drag coefficient with inlet mass-flow ratio and boundary-layer-scoop height for 25°-inlet configuration. Free-stream Mach number, 2.0; canard control-surface deflection angle, 0°.

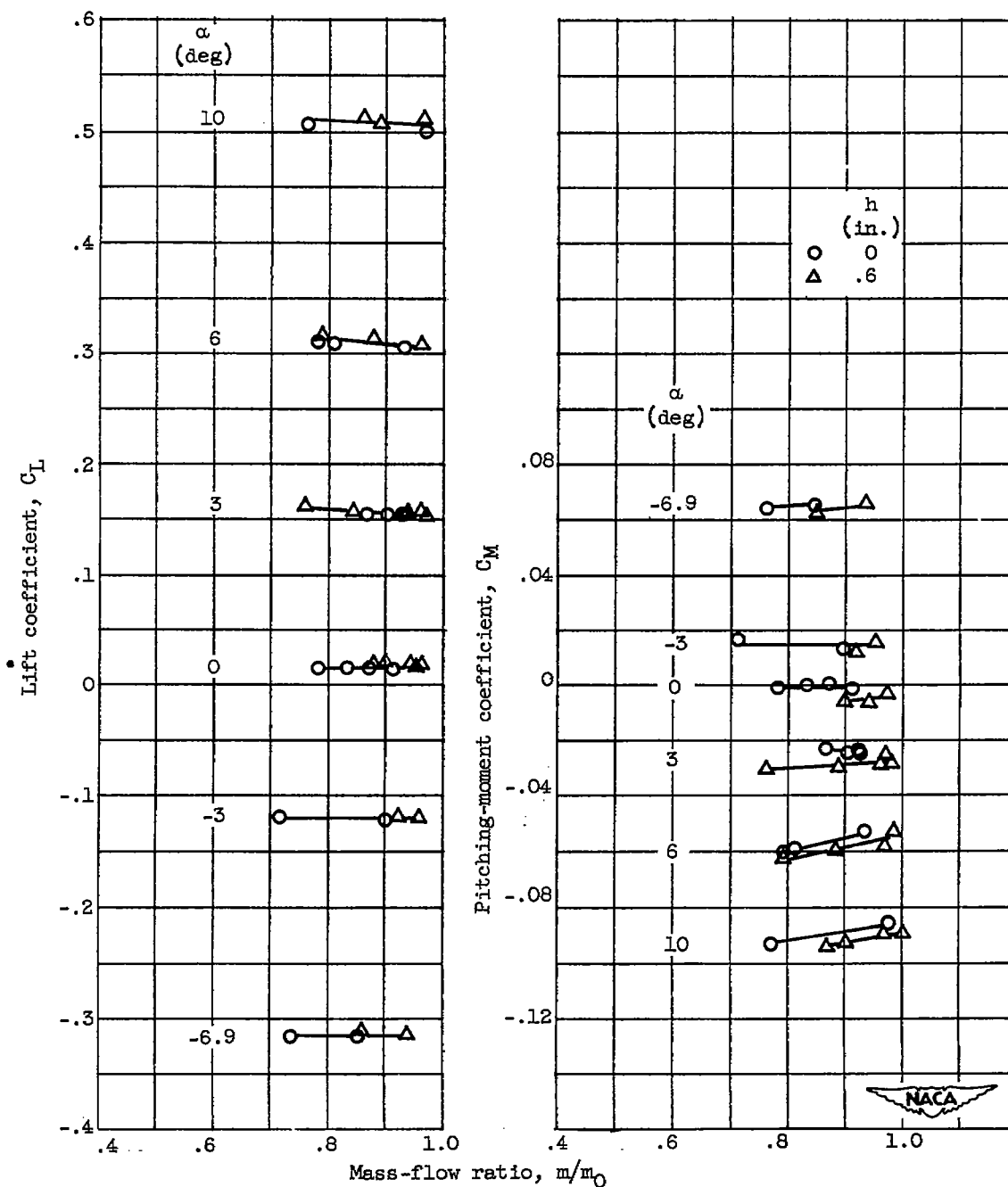
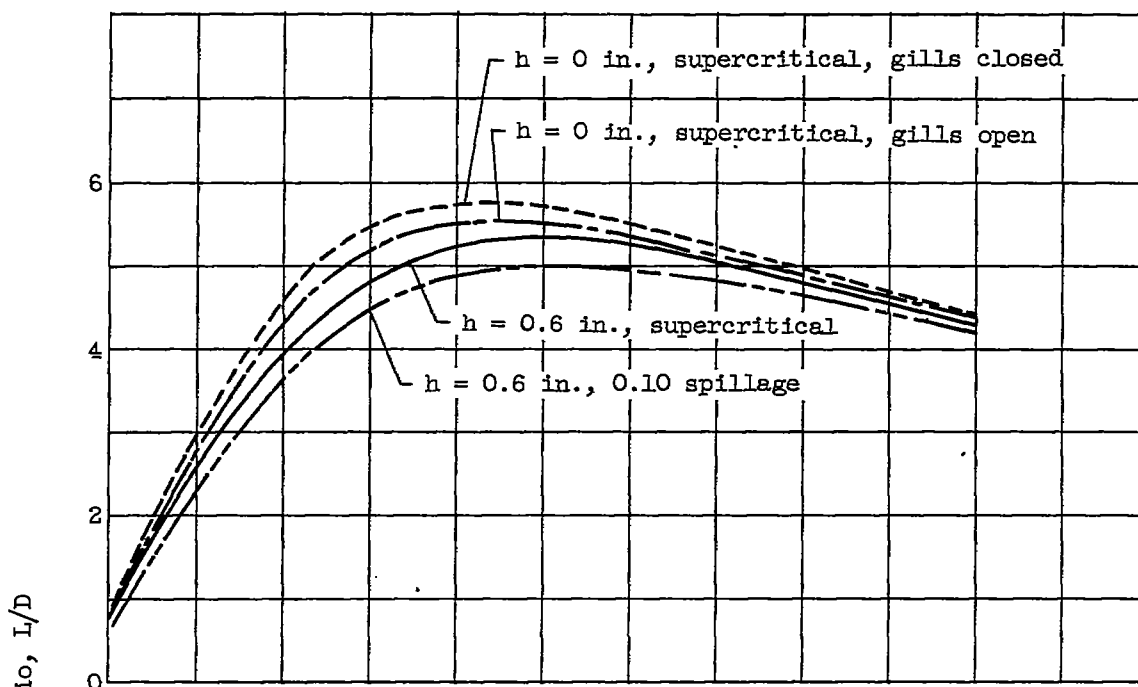
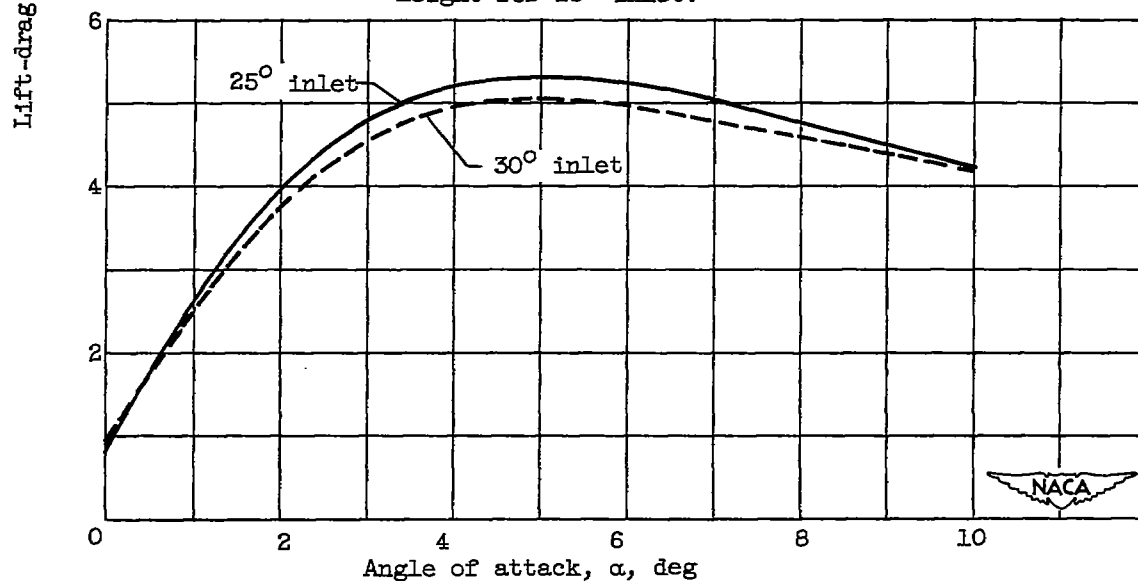


Figure 13. - Variation of lift and pitching-moment coefficients with inlet mass-flow ratio and boundary-layer-scoop height for 25°-inlet configuration. Free-stream Mach number, 2.0; canard control-surface deflection angle, 0°.

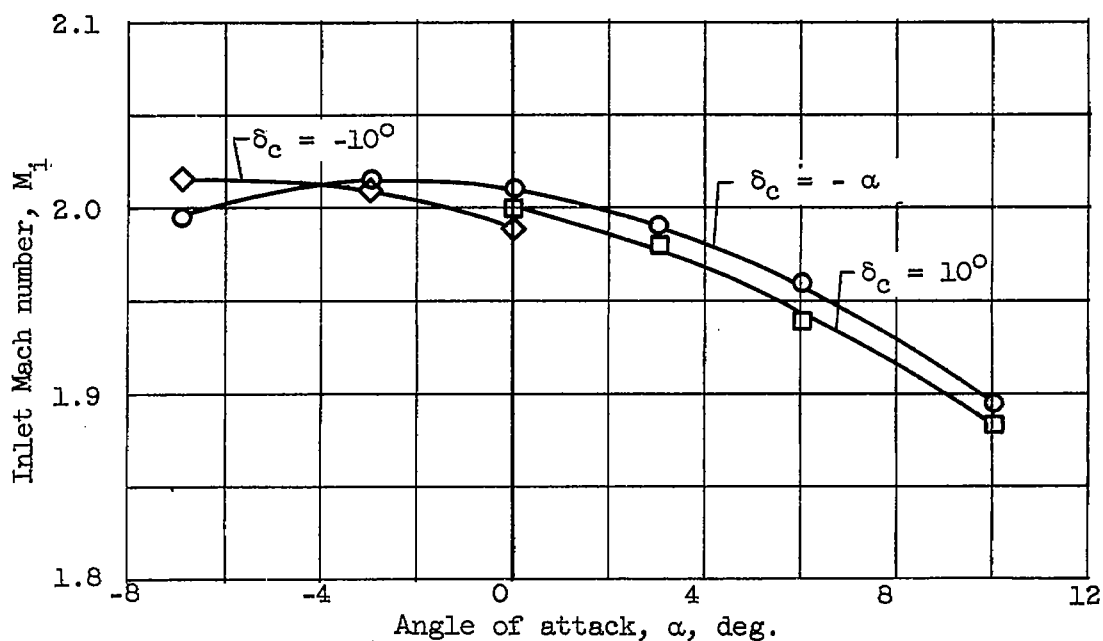


(a) Effect of mass-flow ratio and boundary-layer-scoop height for  $25^\circ$  inlet.

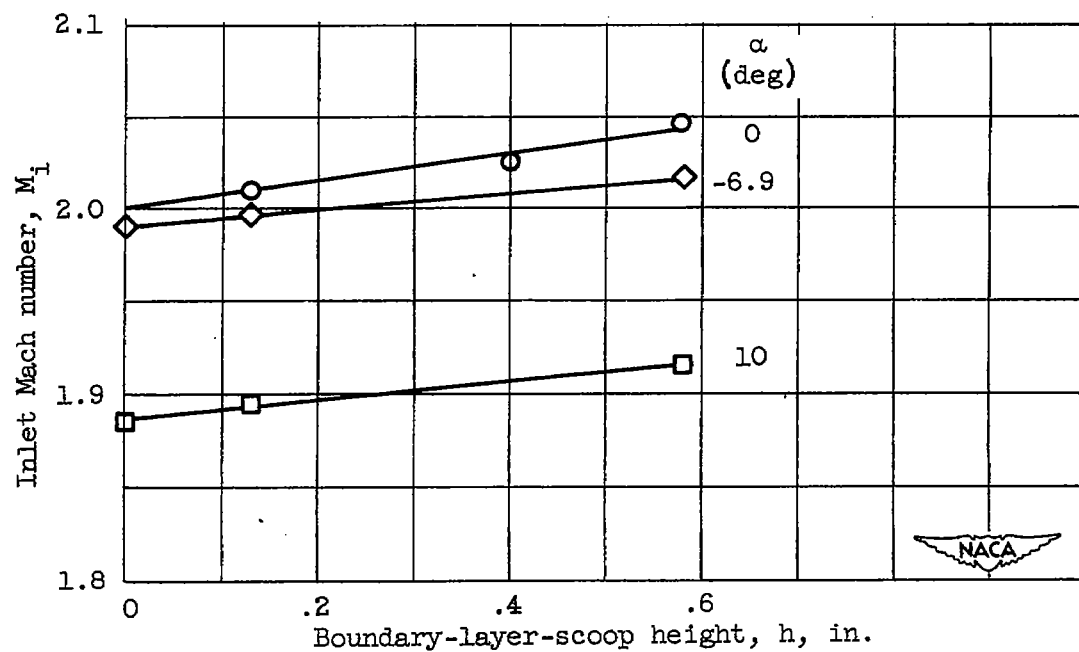


(b) Comparison of  $25^\circ$  and  $30^\circ$  inlets; boundary-layer-scoop-height, 0.6 in.; mass flow, supercritical.

Figure 14. - Effect of test variables on lift-drag ratio. Free-stream Mach number, 2.0; canard control-surface deflection angle,  $0^\circ$ .



(a) Effect of angle of attack; boundary-layer-scoop height  $h$ , 0.13 in.



(b) Effect of ramp position; canard control-surface deflection angle,  $\delta_c$ ,  $-\alpha^\circ$ .

Figure 15. - Inlet Mach number measured with wedge mounted at station 50. Free-stream Mach number, 2.0.

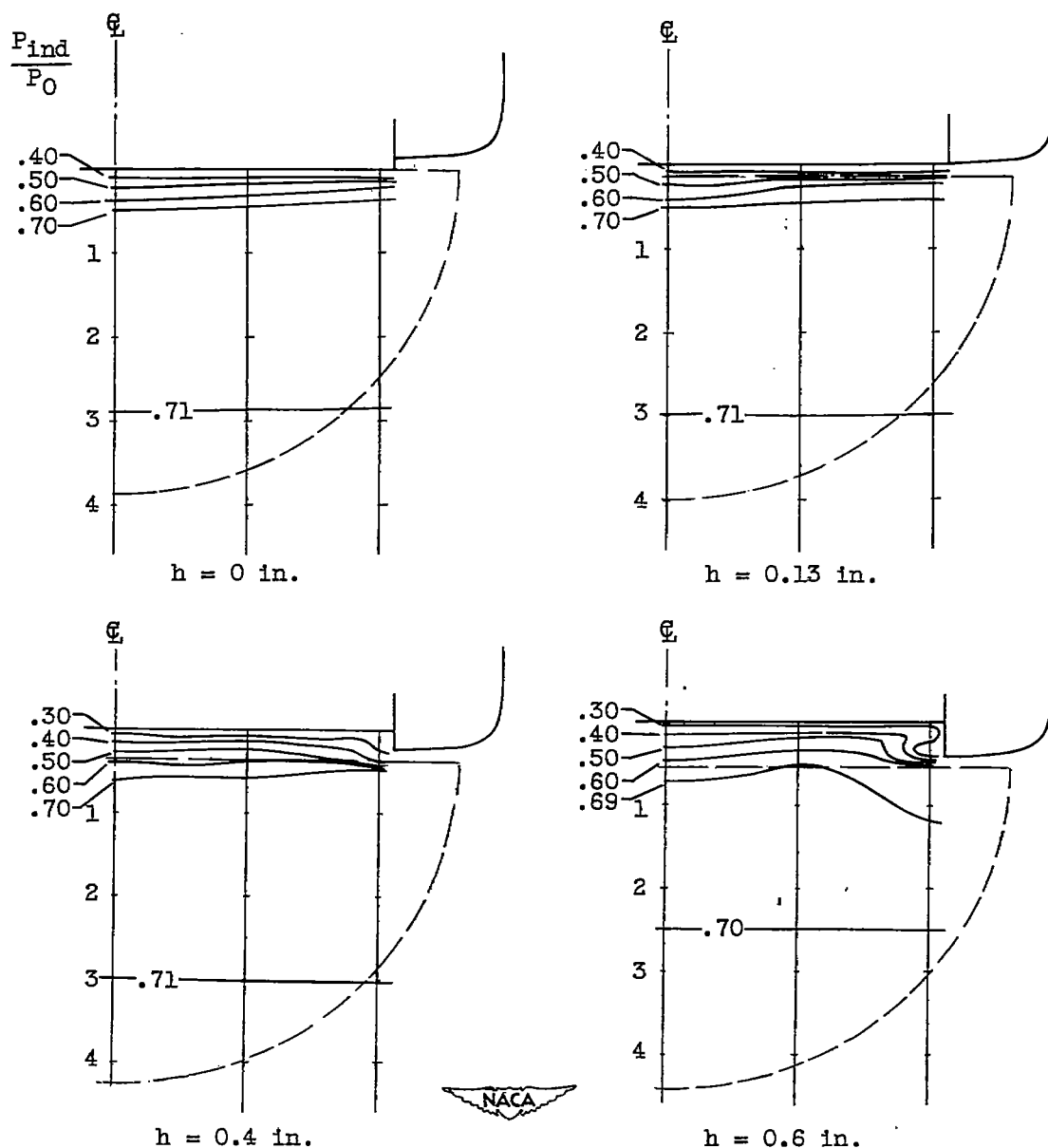
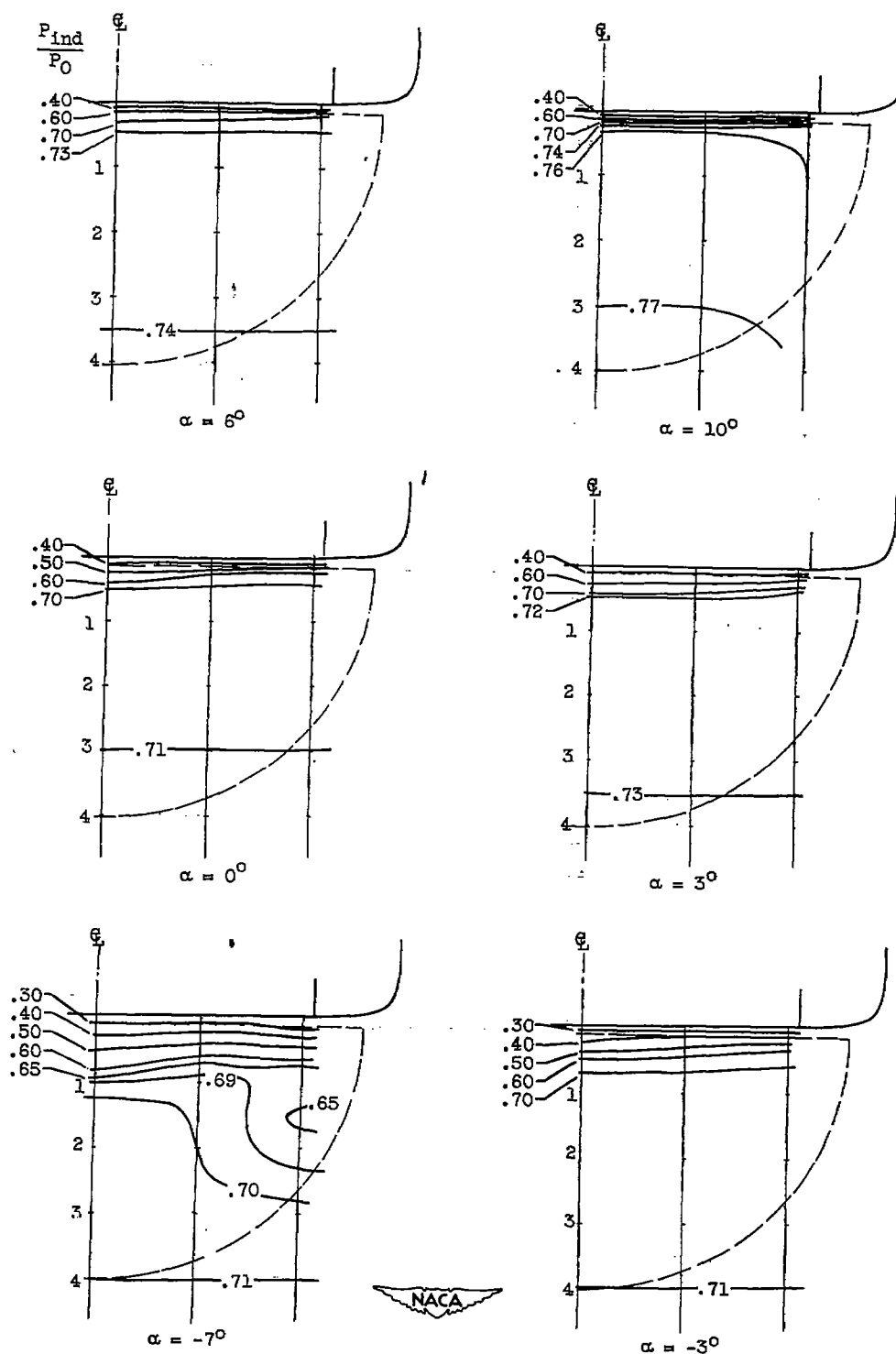


Figure 16. - Effect of ramp position on flow field ahead of inlet. Free-stream Mach number, 2.0; angle of attack,  $0^\circ$ ; canard control-surface deflection angle,  $0^\circ$ .

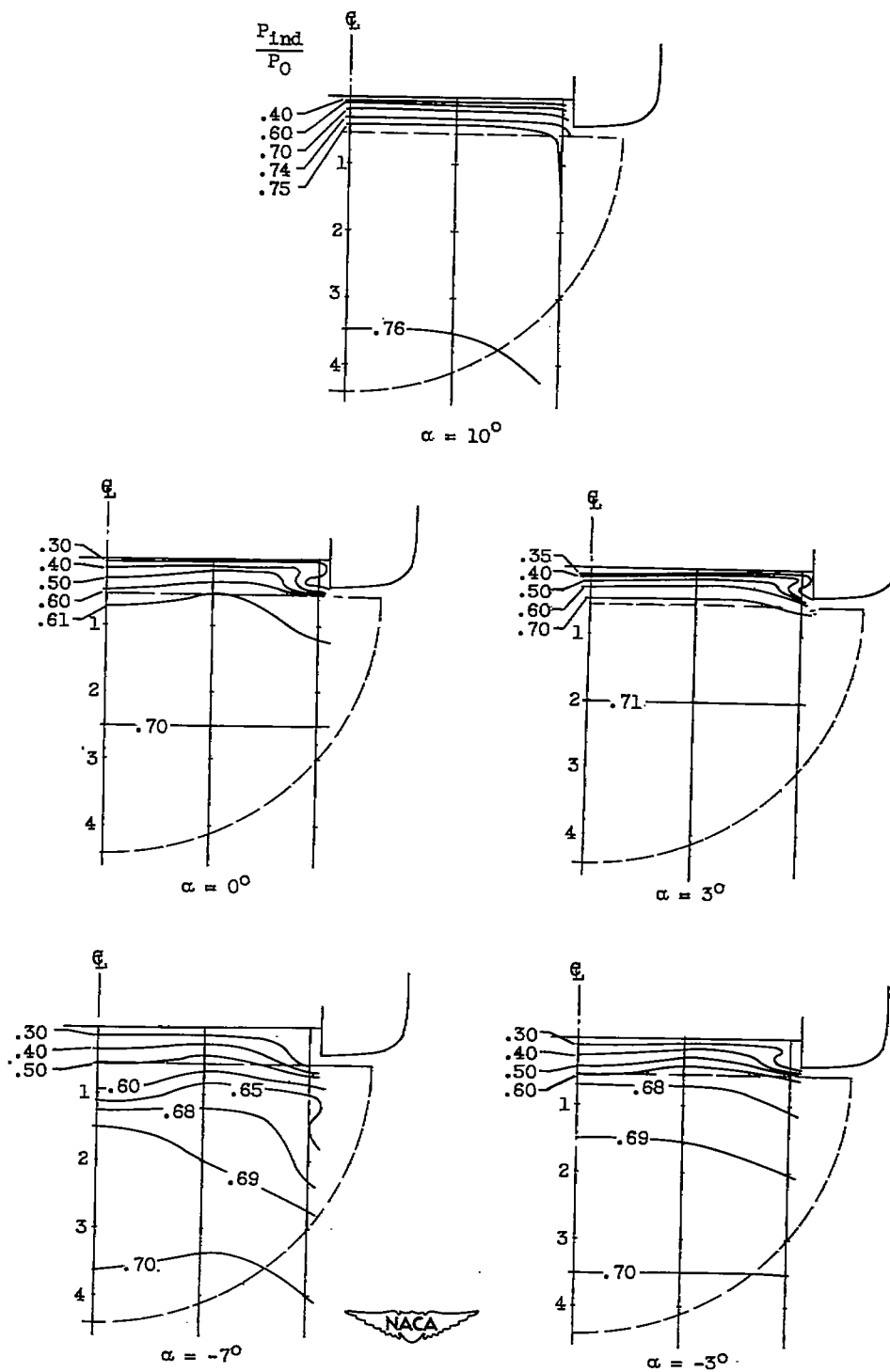




(a) Boundary-layer-scoop height, 0.13 inch.

Figure 17. - Effect of angle of attack on flow field ahead of inlet. Free-stream Mach number, 2.0; canard control-surface deflection angle,  $-\alpha^\circ$ .

2747



(b) Boundary-layer-scoop height, 0.6 inch.

Figure 17. - Concluded. Effect of angle of attack on flow field ahead of inlet. Free-stream Mach number, 2.0; canard control-surface deflection angle,  $-\alpha^\circ$ .

~~CONFIDENTIAL~~

NACA RM E52J22

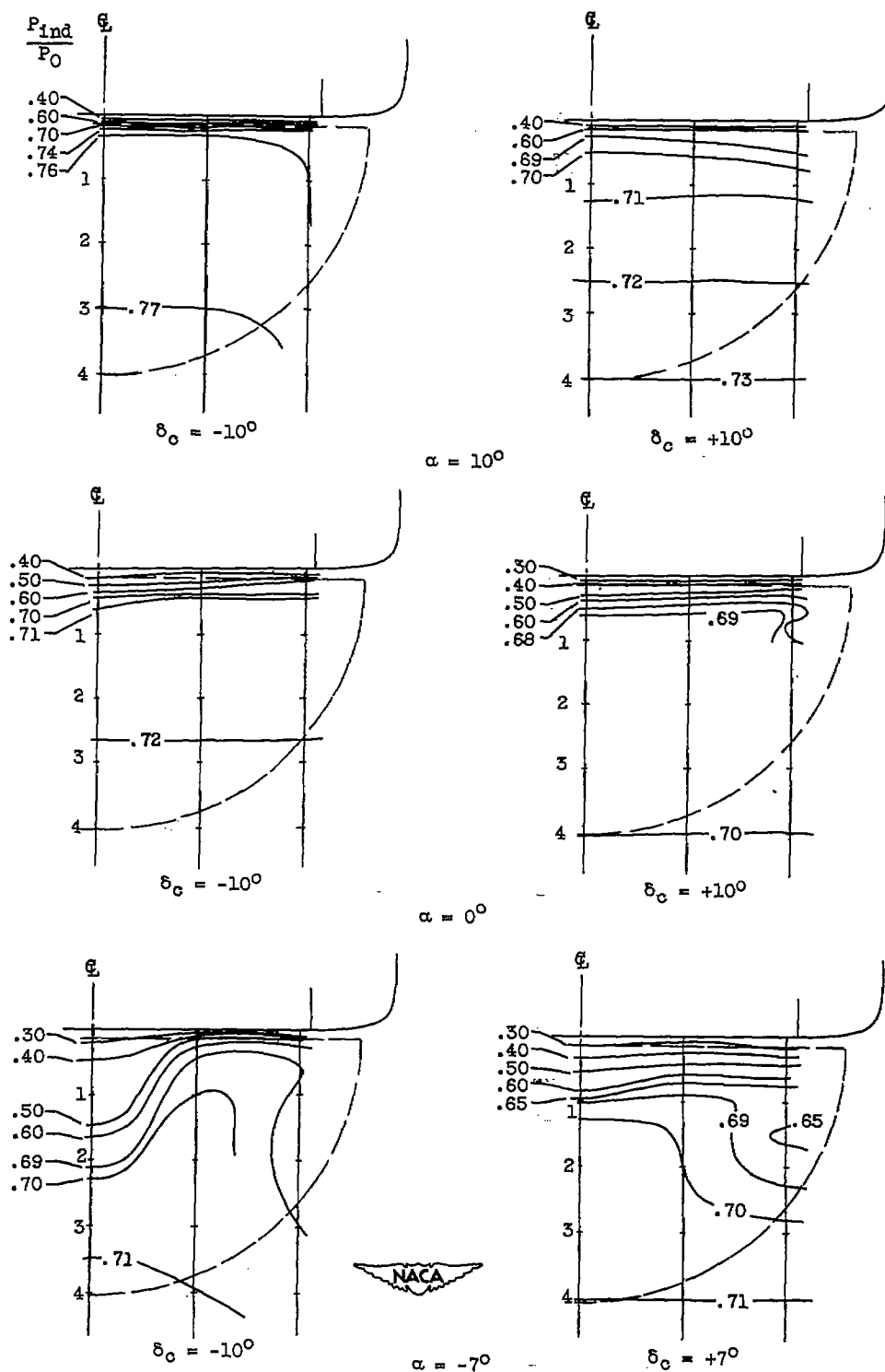


Figure 18. - Effect of canard control-surface deflection angle on flow field ahead of inlet. Free-stream Mach number, 2.0; boundary-layer-scoop height, 0.13 inch.

~~CONFIDENTIAL~~

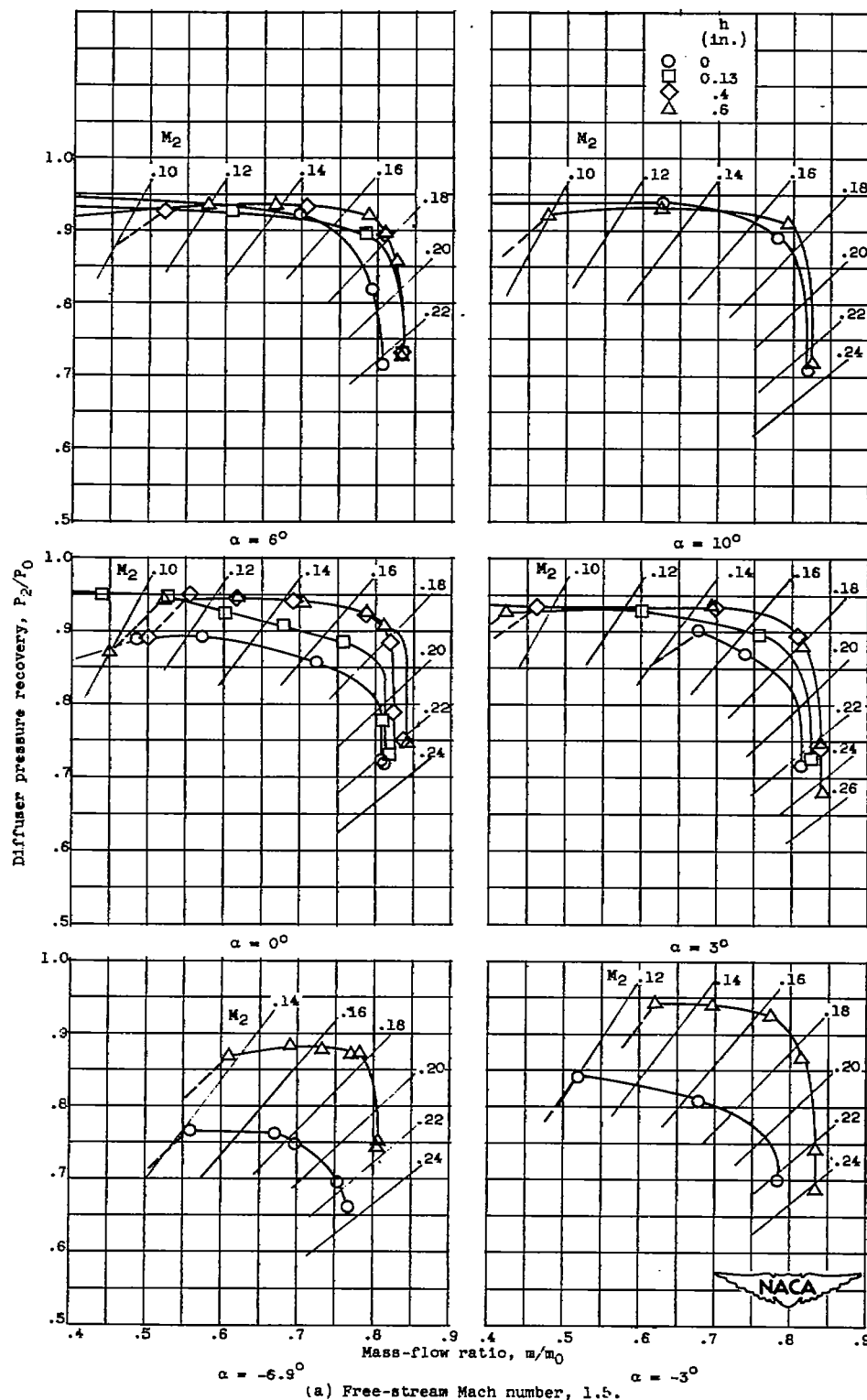


Figure 19. - Variation of diffuser pressure recovery with inlet mass-flow ratio for several boundary-layer-scoop heights and angles of attack for 25°-inlet configuration. Canard control-surface deflection angle, 0°.

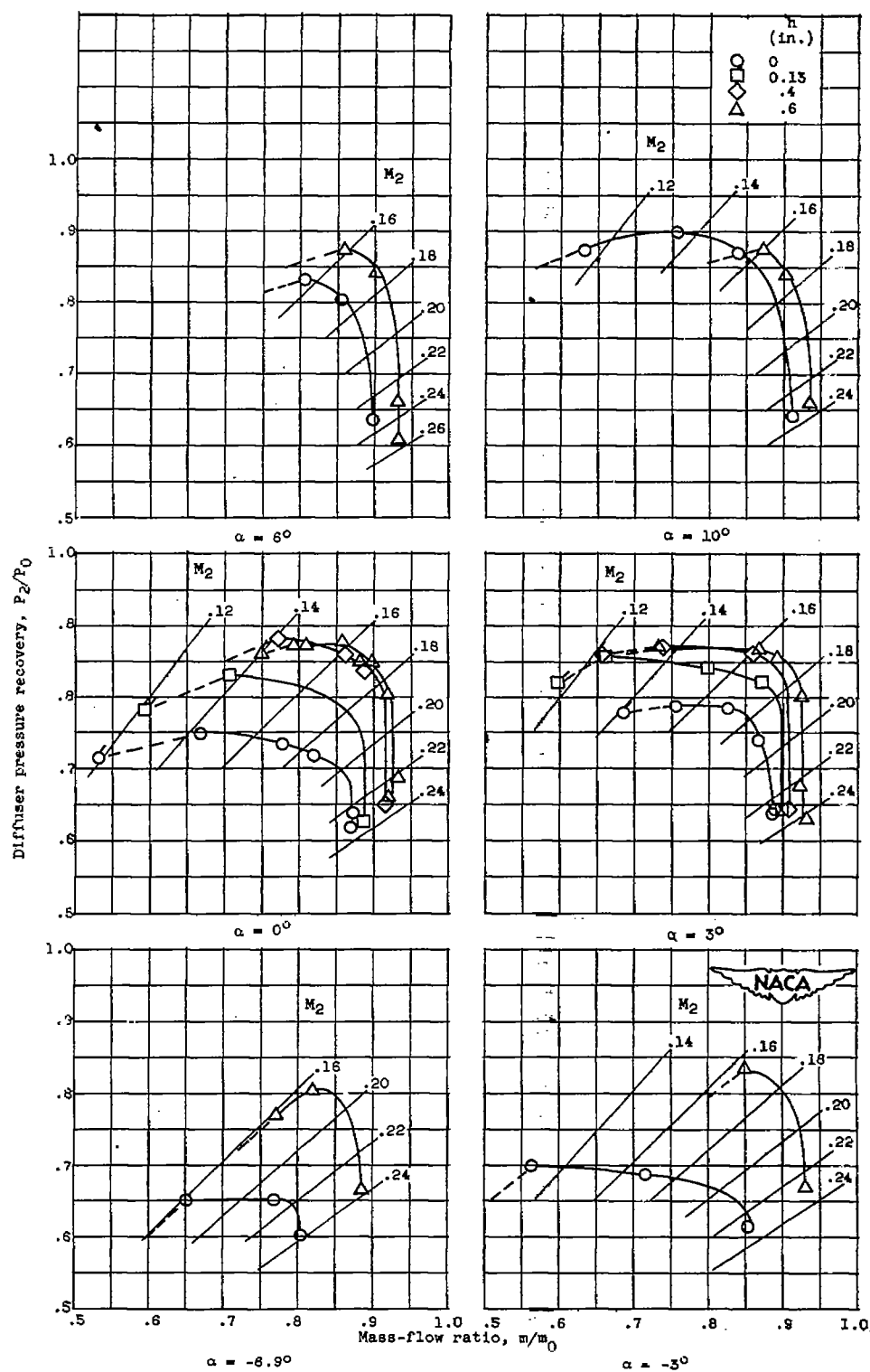
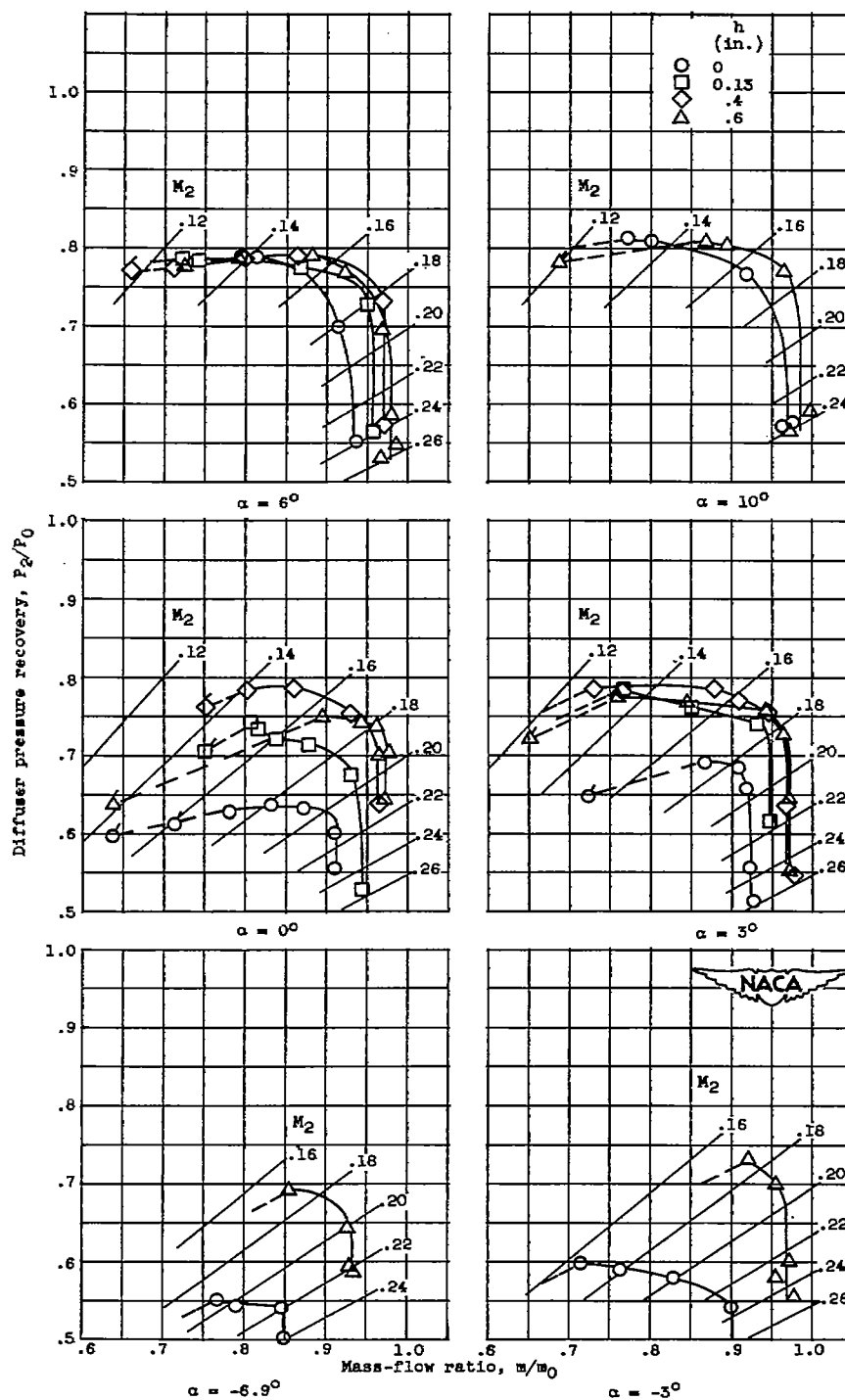
~~CONFIDENTIAL~~

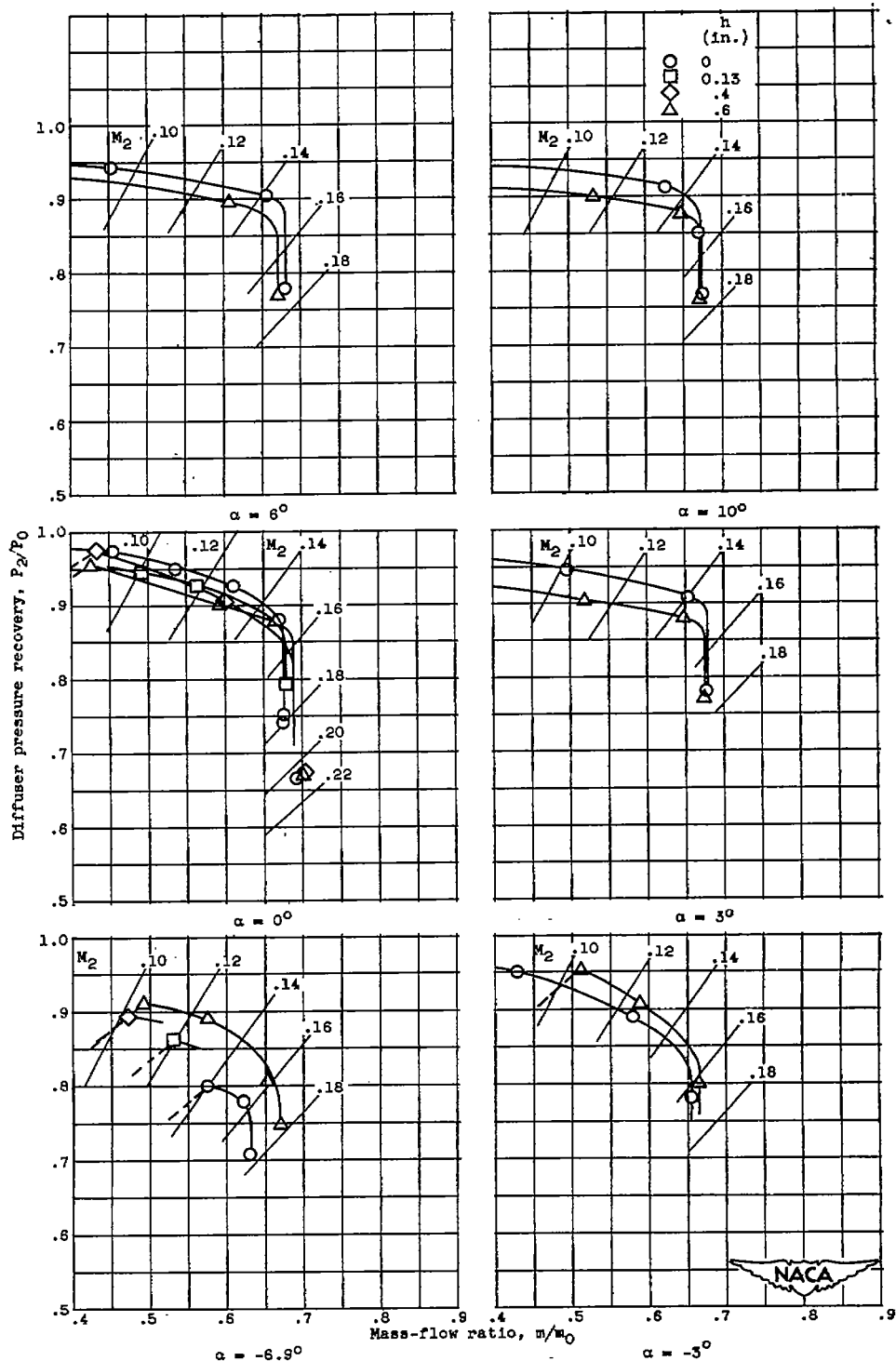
Figure 19. - Continued. Variation of diffuser pressure recovery with inlet mass-flow ratio for several boundary-layer-scoop heights and angles of attack for 25°-inlet configuration. Canard control-surface deflection angle, 0°.

~~CONFIDENTIAL~~



(c) Free-stream Mach number, 2.0.

Figure 19. - Concluded. Variation of diffuser pressure recovery with inlet mass-flow ratio for several boundary-layer-scoop heights and angles of attack for 25°-inlet configuration. Canard control-surface deflection angle, 0°.



(a) Free-stream Mach number, 1.5.

Figure 20. - Variation of diffuser pressure recovery with inlet mass-flow ratio for several boundary-layer-scoop heights and angles of attack for 30°-inlet configuration. Canard control-surface deflection angle, 0°.

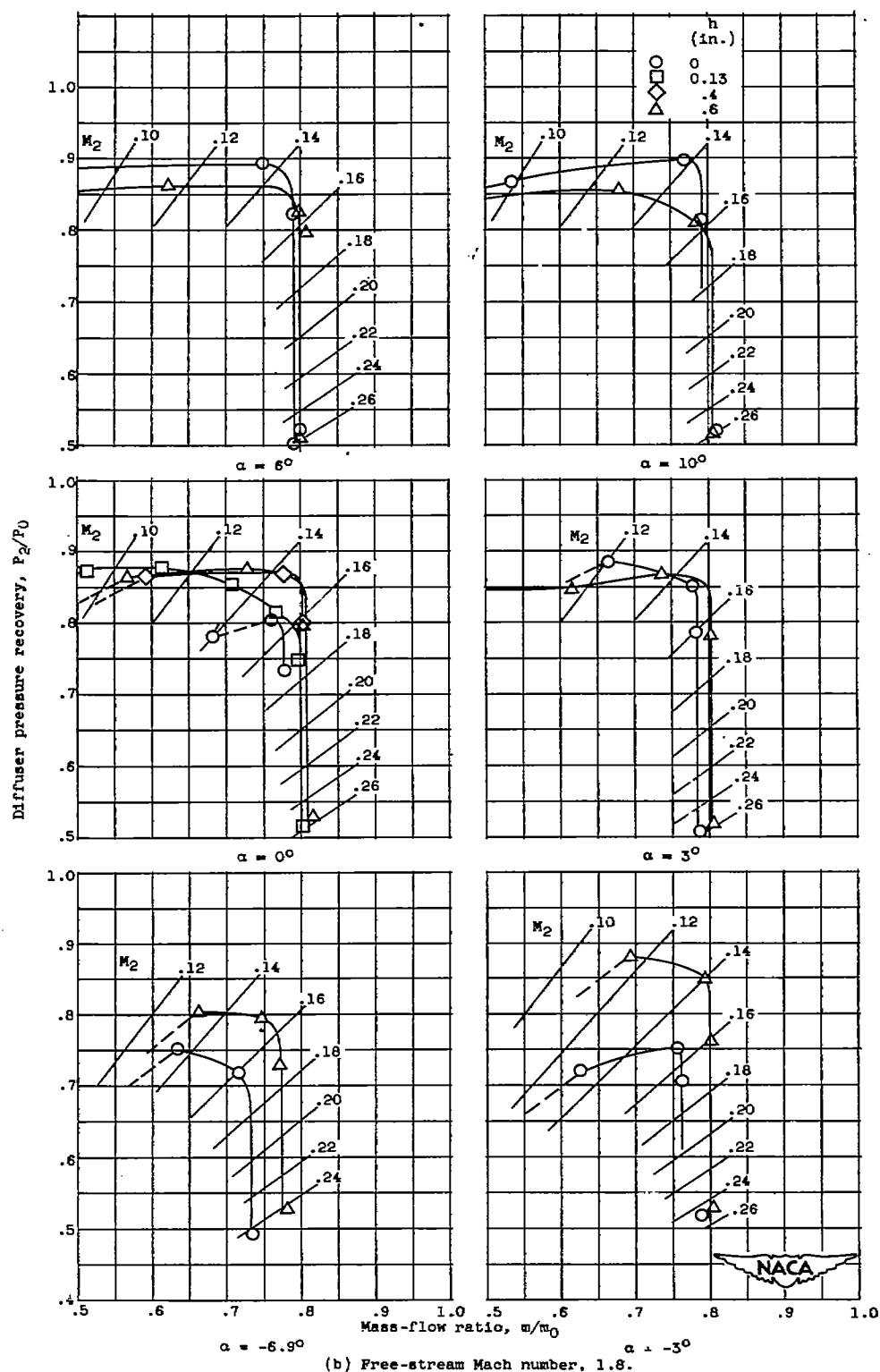


Figure 20. - Continued. Variation of diffuser pressure recovery with inlet mass-flow ratio for several boundary-layer-scoop heights and angles of attack for  $30^\circ$ -inlet configuration. Canard control-surface deflection angle,  $0^\circ$ .



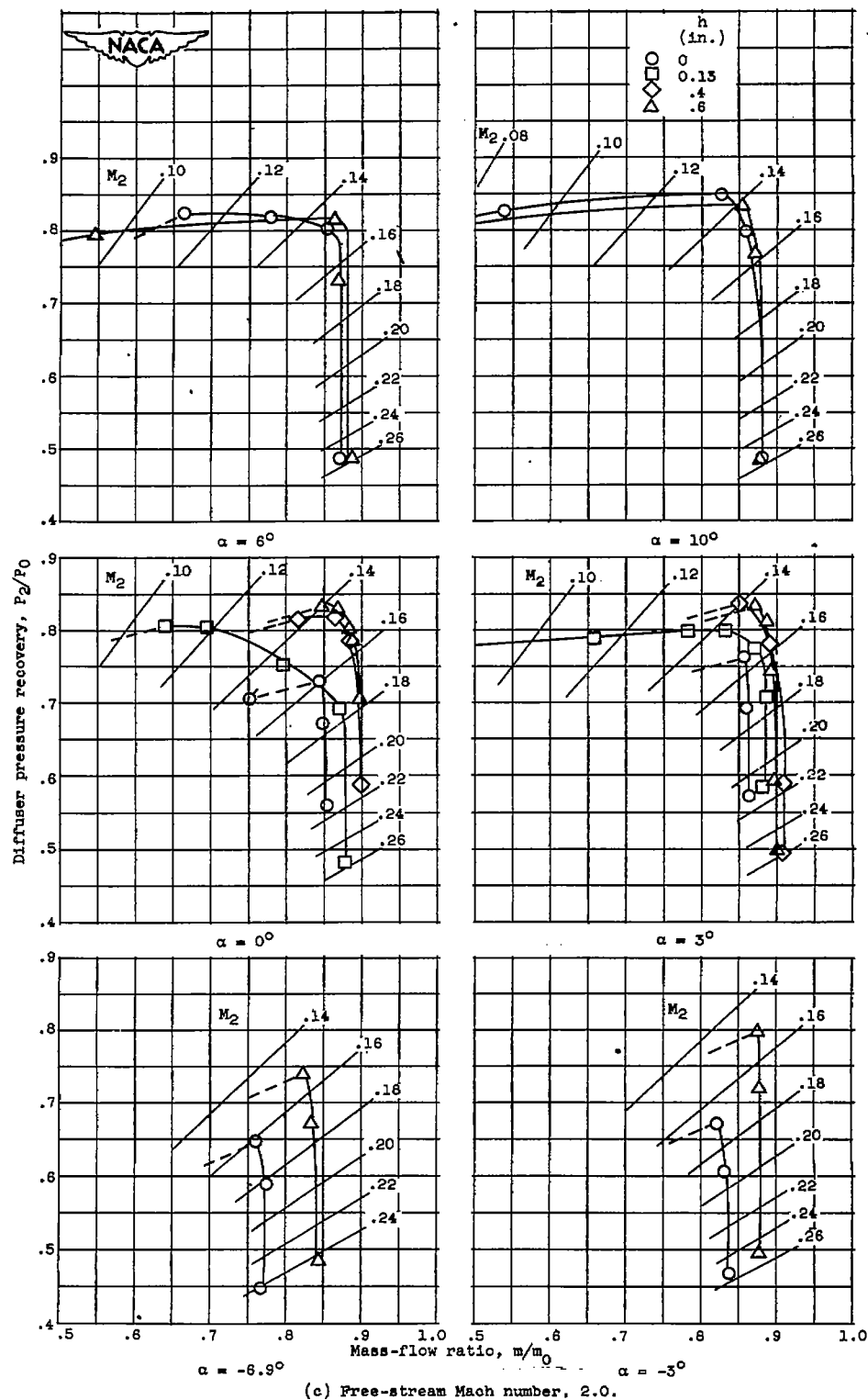


Figure 20. - Concluded. Variation of diffuser pressure recovery with inlet mass-flow ratio for several boundary-layer-scoop heights and angles of attack for 30°-inlet configuration. Canard control-surface deflection angle, 0°.

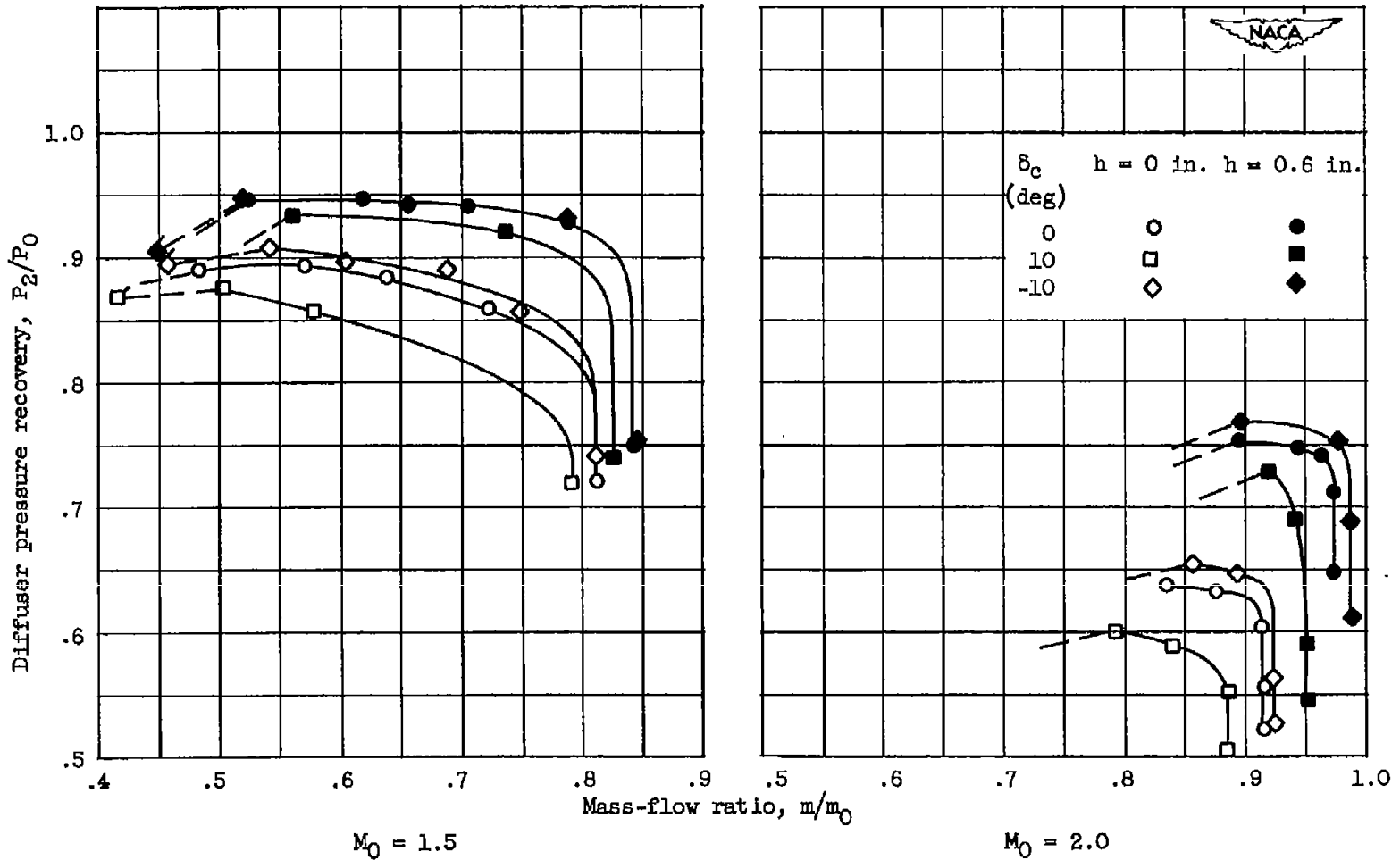


Figure 21. - Effect of canard control-surface deflection angle on diffuser characteristics for 25°-inlet configuration. Angle of attack, 0°.

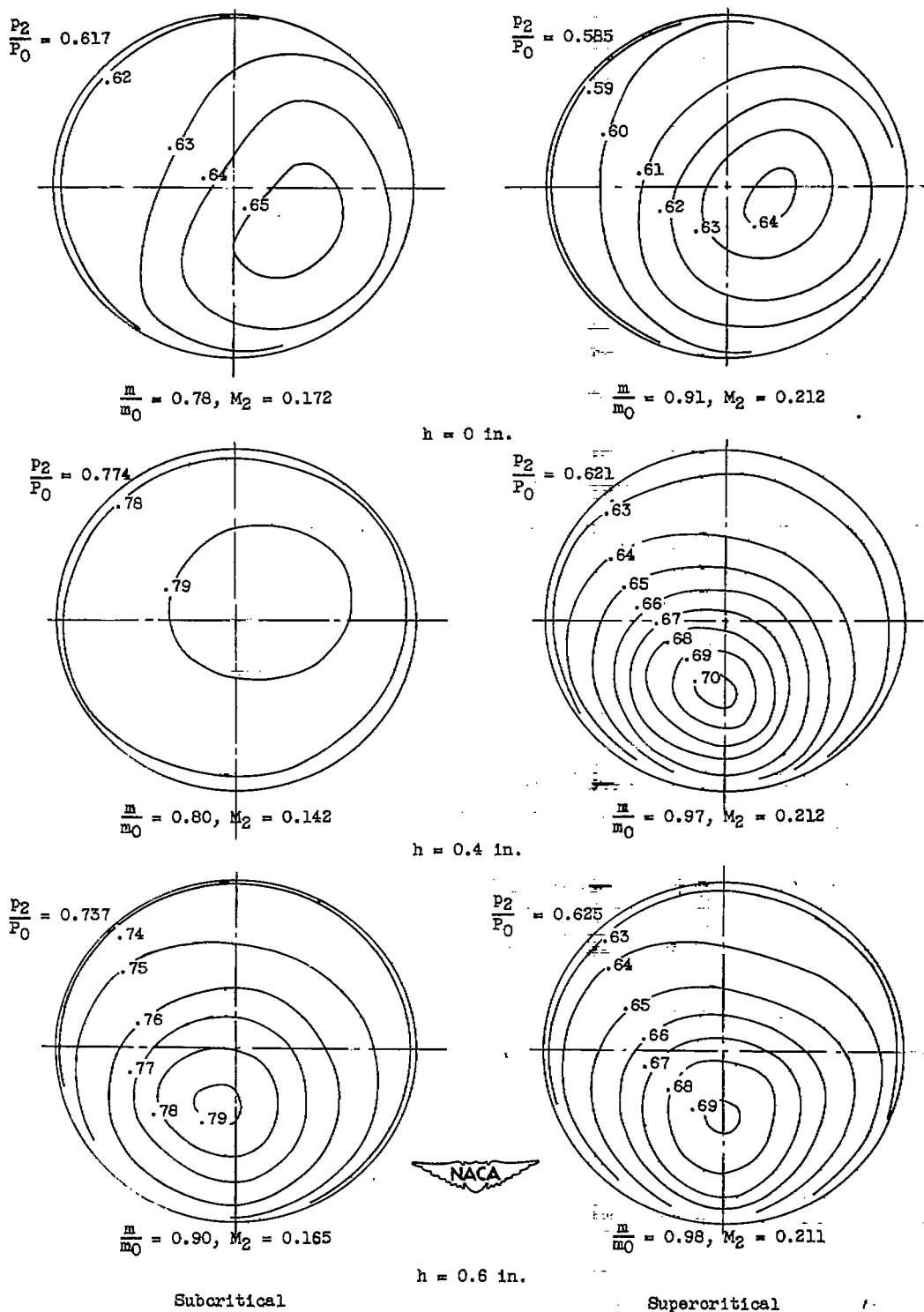


Figure 22. - Effect of mass-flow ratio and boundary-layer-scoop height on diffuser-exit total-pressure contours for 25°-inlet configuration. Free-stream Mach number, 2.0; angle of attack, 0°; canard control-surface deflection angle, 0°.

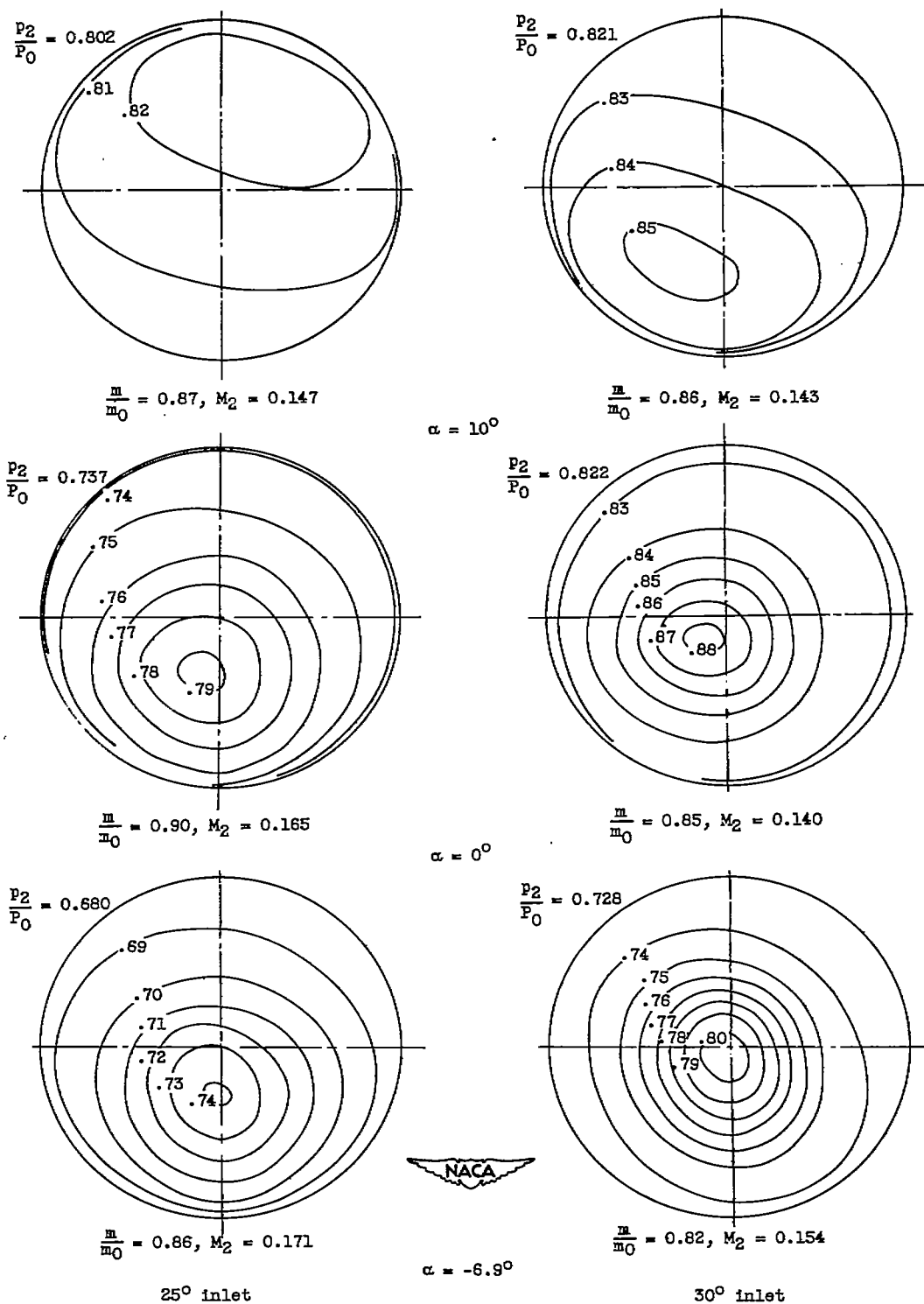


Figure 23. - Effect of angle of attack on diffuser-exit total-pressure contours at maximum pressure recovery. Free-stream Mach number, 2.0; boundary-layer-scoop height, 0.6 inch; canard control-surface deflection angle,  $0^\circ$ .